THE JOURNAL OF BIOLOGICAL CHEMISTRY VOL. 289, NO. 27, pp. 18752–18769, July 4, 2014

Caspase-activated DNase Is Necessary and Sufficient for Oligonucleosomal DNA Breakdown, but Not for Chromatin Disassembly during Caspase-dependent Apoptosis of LN-18 Glioblastoma Cells*

Received for publication, January 13, 2014, and in revised form, May 15, 2014 Published, JBC Papers in Press, May 17, 2014, DOI 10.1074/jbc.M114.550020

María Sánchez-Osuna[1], Mercè Garcia-Belinchón[2], Victoria Iglesias-Guimarais[3], Estel Gil-Guiñón[4], Elisenda Casanelles[1], and Victor J. Yuste[5]

From the Cell Death, Senescence, and Survival Group, Departament de Bioquímica i Biologia Molecular and Institut de Neurociències, Facultat de Medicina, Universitat Autònoma de Barcelona, 08193 Cerdanyola del Vallés, and the Centro de Investigación Biomédica en Red sobre Enfermedades Neurodegenerativas (CIBERNED), 08193 Cerdanyola del Vallés, Barcelona, Spain

Background: DFF40/CAD mediates nuclear fragmentation and oligonucleosomal DNA degradation during apoptosis.
Results: DFF40/CAD overexpression allows apoptotic-defective LN-18 cells to display internucleosomal DNA degradation but not chromatin disassembly upon cytotoxic insult.
Conclusion: DFF40/CAD can induce DNA laddering in the absence of apoptotic chromatin disassembly.
Significance: Dissecting DFF40/CAD regulation may shed light on some of the apparent non-desirable tumor responses in currently used anti-cancer therapies.

Caspase-dependent apoptosis is a controlled type of cell death characterized by oligonucleosomal DNA breakdown and major nuclear morphological alterations. Other kinds of cell death do not share these highly distinctive traits because caspase-activated DNase (DFF40/CAD) remains inactive. Here, we report that human glioblastoma multiforme-derived LN-18 cells do not hydrolyze DNA into oligonucleosomal fragments after apoptotic insult. Furthermore, their chromatin remains packaged into a single mass, with no signs of nuclear fragmentation. However, ultrastructural analysis reveals that nuclear disassembly occurs, although compacted chromatin does not localize into apoptotic nuclear bodies. Caspases become properly activated, and ICAD, the inhibitor of DFF40/CAD, is correctly processed. Using cell-free *in vitro* assays, we show that chromatin from isolated nuclei of LN-18 cells is suitable for hydrolysis into oligonuclesomal fragments by staurosporine-pretreated SH-SY5Y cytoplasms. However, staurosporine-pretreated LN-18 cytoplasms do not induce DNA laddering in isolated nuclei from either LN-18 or SH-SY5Y cells because LN-18 cells express lower amounts of DFF40/CAD. DFF40/CAD overexpression makes LN-18 cells fully competent to degrade their DNA into oligonucleosome-sized fragments, and yet they remain unable to arrange their chromatin into nuclear clumps after apoptotic insult. Indeed, isolated nuclei from LN-18 cells were resistant to undergoing apoptotic nuclear morphology *in vitro*. The use of LN-18 cells has uncovered a previously unsuspected cellular model, whereby a caspase-dependent chromatin package is DFF40/CAD-independent, and DFF40/CAD-mediated double-strand DNA fragmentation does not warrant the distribution of the chromatin into apoptotic nuclear bodies. The studies highlight a not-yet reported DFF40/CAD-independent mechanism driving conformational nuclear changes during caspase-dependent cell death.

Apoptosis is a genetically controlled cell death program in which the condensation of the nucleus and its fragmentation into smaller pieces are the most noticeable features. Another typical trait of apoptotic cell death is the extensive hydrolysis of nuclear DNA into oligonucleosome-sized fragments. These are highly distinctive events (hallmarks) of apoptosis, and no other types of cell death provoke such cellular alterations (1). The nuclei of cells committed to apoptosis undergo different ultrastructural stepwise modifications. In the first stage, chromatin condenses around the nuclear membrane, known as stage I chromatin condensation or stage I nuclear morphology (2). Later nuclear changes include shrinkage and fragmentation of the nucleus into highly packed round masses of condensed chromatin (3, 4), also known as stage II chromatin condensation (2). In parallel, the genomic content is extensively fragmented in a two-step process, in which the DNA is first cleaved into 50–300-kilobase pair (kbp) fragments, an event also

* This work was supported by Ministerio de Economía y Competitividad/Fondo Europeo de Desarrollo Regional (MINECO/FEDER) Grant SAF2012-31485 and Generalitat de Catalunya Grant SGR2009-346.
[1] Formación de Personal Universitario (FPU) fellows from the Ministerio de Ciencia e Innovación (MICINN).
[2] Recipient of Formación de Personal Investigador Fellowship BES-2099-028572 from the Ministerio de Ciencia e Innovación).
[3] Supported by a fellowship from Agència de Gestió d'Ajuts Universitaris i de Recerca (AGAUR, Generalitat de Catalunya).
[4] Held Postdoctoral Contract TRA2009-0185 from the Ministerio de Ciencia e Innovación. Present address: Instituto de Biología Molecular de Barcelona, CSIC, C/Baldiri i Reixac 20, Barcelona 08028, Spain.
[5] Supported by the Ramón y Cajal Program (Ministerio de Educación y Ciencia). To whom correspondence should be addressed: Departament de Bioquímica i Biologia Molecular, Facultat de Medicina, Campus de Bellaterra, 08193 Bellaterra, Cerdanyola del Vallès, Barcelona, Spain. Tel.: 34-93-581-3762; Fax: 34-93-581-1573; E-mail: victor.yuste@uab.cat.

known as high molecular weight (HMW)[6] DNA degradation, followed by hydrolysis into smaller fragments of oligonucleosomal size, also called "DNA ladder" (5, 6). The molecular machinery involved in the apoptotic hallmarks is a family of cysteine proteases called caspases. Caspases can be broadly classified into "initiator" (caspase-2, -8, -9, and -10) or "effector" caspases (caspase-3, -6, and -7) (7). After direct activation by initiator caspases, effector caspases execute limited proteolysis of downstream specific substrates, triggering a cascade of events that will dismantle the cell (8). The inhibition of caspases in damaged cells avoids cell death as well as apoptotic hallmarks (9, 10).Whereas HMW DNA degradation and stage I nuclear morphology are caspase-independent events (10), oligonucleosomal DNA degradation together with stage II nuclear morphology are considered the hallmarks of caspase-dependent apoptosis (11). The main protein triggering the two hallmarks of apoptotic cell death downstream of the activation of caspases is a nuclease called DNA fragmentation factor 40-kDa subunit (DFF40) (12) or caspase-activated nuclease (13) in humans, or caspase-activated DNase (CAD) (14) in mice. DFF40/CAD remains inactive when combined with its chaperone-inhibitor, ICAD (15), also known as DNA fragmentation factor, 45-kDa subunit (DFF45) (5). After apoptotic insult, active caspase-3 processes ICAD into two aspartic residues, Asp-117 and Asp-224, in both long (DFF45/$ICAD_L$) and short (DFF35/$ICAD_S$) splicing variants (5). The hydrolysis of DFF45/$ICAD_L$ in these two residues allows the release and activation of DFF40/CAD (12, 15). The DNA laddering appears after DFF40/CAD-mediated DNA hydrolysis at internucleosomal sites (12–14). Many approaches have been used to unravel the molecular mechanisms implicated in the onset and progression of apoptotic nuclear morphology and DNA degradation during apoptosis. Classically, stage II chromatin condensation and oligonucleosomal DNA degradation were considered concomitant events (16–19). DFF40/CAD activity still remains as the key biochemical feature triggering both apoptotic nuclear changes and DNA laddering. Yet, some cellular models, in which stage II nuclear morphology occurs in the absence of DNA laddering, have recently pointed out that these two apoptotic hallmarks can be dissociated (20–23). Moreover, no cellular models have so far been reported showing the presence of DNA ladder in the absence of nuclear disassembly following caspase-dependent apoptotic cell death.

In this study, we report on a glioblastoma multiforme-derived human cell line, LN-18 cells, in which apoptotic stimuli induce caspase-dependent cell death, characterized by a single mass of highly compacted chromatin without displaying either oligonucleosomal DNA degradation or stage II nuclear morphology. The poor expression of DFF40/CAD endonuclease seems to be the reason why LN-18 cells cannot generate DNA laddering after apoptotic stimuli, as the overexpression of the nuclease is sufficient to make these cells fully competent to degrade DNA into oligonucleosome-sized fragments. Interestingly, we show that higher levels of DFF40/CAD failed to induce stage II apoptotic nuclear morphology after caspase-dependent cytotoxic insult. Moreover, by using cell-free assays, we demonstrate that LN-18 isolated nuclei cannot display apoptotic nuclear alterations. Altogether, our results show, for the first time, that DFF40/CAD is necessary and sufficient to generate DNA laddering, but not sufficient to provoke nuclear disassembly during apoptosis, and other players seem to be needed.

EXPERIMENTAL PROCEDURES

Reagents—All chemicals were obtained from Sigma-Aldrich unless otherwise indicated. The pan-caspase inhibitor q-VD-OPh was from MP Biomedicals Europe (Illkirch, France). Antibodies against caspase-3 (9662; 1:2,000) and caspase-7 (9492; 1:2,000) were purchased from Cell Signaling Technology (Beverly, MA). Antibodies against DFF40/CAD (AB16926, 1:500) and α-fodrin (clone AA6) (MAB1622; 1:40,000) were obtained from Millipore. Antibodies against caspase-6 (clone 3E8) (M070-3; 1:2,000) and DFF45/ICAD (clone 6B8) (M037-; 1:40,000) were from MBL (Naka-ku Nagoya, Japan). Anti-lamin A/C (clone JOL2) (Ab40567; 1:2,000) was from Abcam (Cambridge, UK). Anti-p23 antibody (clone JJ3) (NB300-576; 1:10,000) was obtained from Novus Biological Europe, Inc. (Cambridge, UK). Horseradish peroxidase-conjugated secondary antibodies against mouse IgG (A9044; 1:20,000) or rabbit IgG (A0545; 1:20,000) were purchased from Sigma. The cytotoxic drugs used were actinomycin D (50 μM as lethal dose, 40 nM as a sublethal dose), cytosine arabinoside (2,500 μg/ml), azacytidine (100 μM); bevacizumab (500 μg/ml), camptothecin (100 μM), ceramide-2 (50 μM), ceramide-8 (50 μM), cisplatin (50 μg/ml), colchicine (50 μM), curcumin (100 μM), cycloheximide (100 μM), diamide (750 μM), doxorubicin (100 μM), epigallocatechin (500 μM), ergocalciferol (100 μM), etoposide (100 μM), 5-fluorouracil (1000 μM), gencitabine (300 μM), GW4869 (100 μM), rinotecan (500 μM), methotrexate (500 μM), MG132 (20 μM), nocodazole (100 μM), oxaliplatin (100 μg/ml), paclitaxel (50 μM), rotenone (100 μM), staurosporine (STP, 1 μM), temozolomide (50 μM), vinblastine (25 μM), CH11 (0.1 μg/ml), TNFα (0.1 μg/ml), and TRAIL (0.1 μg/ml).

Cell Lines and Culture Procedures—IMR-5, LN-18, and SH-SY5Y cells were routinely grown in 100-mm culture dishes (BD Falcon, Madrid, Spain) containing 10 ml of Dulbecco's modified Eagle's medium (DMEM) supplemented with penicillin/streptomycin (100 units/ml and 100 μg/ml, respectively) and 10% of heat-inactivated fetal bovine serum (FBS) (Invitrogen). Medium was routinely changed every 3 days. Cells were maintained at 37 °C in a saturating humidity atmosphere containing 95% air and 5% CO_2.

Chromatin Staining with Hoechst 33258 and Trypan Blue Exclusion Assays—Nuclear morphology staining with Hoechst 33258 and trypan blue assays were performed as established previously in our laboratory (24). Cell nuclei were visualized with a Nikon ECLIPSE TE2000-E microscope equipped with epifluorescence optics under UV illumination and a Hamamatsu ORCA-ER photographic camera. Stained nuclei

[6] The abbreviations used are: HMW, high molecular weight; CAD, caspase-activated DNase; DEVD, Asp-Glu-Val-Asp DFF40/CAD, DNA fragmentation factor, 40-kDa subunit; DFF45, DNA fragmentation factor, 45-kDa subunit; ICAD, inhibitor of CAD; LDH, lactate dehydrogenase; LMW, low molecular weight; MTT, 3-(4,5-dimethylthiazol-2-yl)-2,5-diphenyltetrazolium bromide; qVD, Q-VD-OPh, *N*-(2-quinolyl)valyl-aspartyl-(2,6-difluorophenoxy)-methyl ketone; STP, staurosporine; TRAIL, TNF-related apoptosis-inducing ligand.

were scored as stage I (partial chromatin condensation in the absence of karyorrhexis), stage II (nuclear pyknosis and karyorrhexis), or stage III (nuclei shrinkage and highly compacted chromatin) morphology (10).

Cell Viability through MTT Reduction Assay—MTT is a water-soluble tetrazolium salt that can be reduced only by metabolically viable cells. The result is a colored water-insoluble formazan salt. This technique was performed as described previously (18).

Cell Death through Lactate Dehydrogenase (LDH) Release Assay—The measure of extracellular LDH was performed by a modified protocol from Decker and Lohmann-Matthes (25). Cells were seeded in a 96-multiwell plate at 50% confluence the day before treatment. Then, medium was replaced by 50 μl of fresh medium containing or not 1 μM STP. 24 h later, 20 μl of lactate solution (14.38 mg/ml in 10 mM Tris buffer, pH 8.5) was added, followed by 20 μl of INT solution (0.9 mg/ml INT in PBS prepared from a 20 mg/ml stock solution in dimethyl sulfoxide). The enzymatic reaction was started by addition of 20 μl of a PBS solution containing NAD^+ (1.65 mg/ml), diaphorase ($7{\cdot}10^{-7}$ units/ml), BSA (0.015%), and sucrose (0.6%) and allowed to proceed for 20 min. The reaction was stopped by the addition of 20 μl of the LDH inhibitor oxamate (5.6 mg/ml in PBS). Absorbance was measured by using a 490 nm filter in a BIO-TEK FL800 fluorometer (Izasa, Spain). The percentage of LDH activity in the culture medium was calculated taking into account the LDH activity obtained from non-treated cells permeabilized with a solution containing 1% Triton X-100, assumed as 100% of LDH activity.

Low Molecular Weight (LMW) or Oligonucleosomal DNA Degradation Analysis—LMW analysis was carried out as described previously (26). Extracted DNA was analyzed in 1.8% agarose gel in 1 mM EDTA, 40 mM Tris acetate, pH 7.6, stained in 0.5 μg/ml ethidium bromide, and then visualized using a Syngene Gene Genius UV transilluminator equipped with a photographic camera.

HMW DNA Fragmentation Analysis—Detection of HMW fragments was made as described previously (23). The gel was electrophoresed at room temperature for 16 h at 45 V. Following electrophoresis, the gel was stained in 2 μg/ml ethidium bromide for 2 h and washed twice with distilled water for 30 min. DNA was visualized using a Syngene Gene Genius UV transilluminator coupled with a photographic camera.

Transmission Electron Microscopy—Transmission electron microscopy was used to examine the nuclear morphology of IMR-5, SH-SY5Y, and LN-18 cells as well as LN-18 cells transfected with pcDNA3.1 containing or not the open reading frame of the human CAD. Stably transfected cells were left untreated or treated with staurosporine for 10 h. Cells were then collected and fixed with 2.5% (v/v) glutaraldehyde and 2% (v/v) paraformaldehyde (EM grade, Merck, Darmstadt, Germany) in phosphate buffer (100 mM, pH 7.4). After fixation, pellets were rinsed four times with phosphate buffer and post-fixed in 1% (w/v) osmium tetroxide (TAAB Laboratories, Berkshire, UK) containing 0.8% (w/v) potassium hexacyanoferrate (III) (Sigma) for 2 h. After four washes with deionized water, pellets were sequentially dehydrated in acetone. All of these steps were performed at 4 °C. Samples were then embedded in Eponate 12™ resin (Ted Pella Inc., Redding, CA) and polymerized for 48 h at 60 °C. Ultrathin (70 nm thick) sections were placed on noncoated copper grids (200 meshes), contrasted with uranyl acetate and lead citrate solutions, and visualized with a transmission electron microscope (Jeol JEM-1400) equipped with a CCD GATAN ES1000W Erlangshen camera.

DEVD-directed Caspase Activity—Quantitative DEVD-like activities in cell lysates were performed as described previously (27). The resulting 96-multiwell microplates were incubated for 10 h at 35 °C. The data were obtained by using a BIO-TEK Synergy HT fluorometer, under an excitation filter of 360 nm (40-nm bandwidth) and an emission filter of 530 nm (25-nm bandwidth).

Protein Extractions and Western Blotting—Cells were detached, pelleted at 600 × *g* for 5 min, and washed once with PBS. Then cells were lysed 15 min on ice with Igepal buffer (50 mM Tris-HCl, pH 6.8, 1 mM EDTA, 150 mM NaCl, 1% Igepal CA-630, 1× protease inhibitor cocktail (Sigma)) for cytosolic protein extracts. The pellets were clarified by centrifuging at 16,000 × *g* for 5 min at 4 °C. Alternatively, cells were lysed with SET buffer (10 mM Tris-HCl, pH 6.8, 150 mM NaCl, 1 mM EDTA, 1% SDS) and heated at 95 °C for 10 min to obtain total protein extracts. The protein concentration in the supernatants was quantified by a modified Lowry assay (DC protein assay; Bio-Rad), and 20–35 μg of protein was loaded in SDS-polyacrylamide gels. Proteins were electrophoresed and electrotransferred onto polyvinylidene difluoride (PVDF) Immobilon-P membrane (Millipore) or Protran nitrocellulose transfer membrane (Whatman). After blocking with Tris-buffered saline (TBS), 0.1% Tween 20 containing 5% nonfat dry milk, the membranes were probed with the appropriate specific primary antibodies and incubated with the adequate secondary antibodies conjugated with peroxidase. Finally, immunoblots were developed by EZ-ECL chemiluminescence detection kit (Biological Industries, Kibbutz Beit-Haemek, Israel). When the specific antibodies were blotted, the membranes were stained for 5 min in a solution containing 10% methanol, 2% acetic acid, and 0.1% naphthol blue. Then, membranes were destained in a 10% methanol and 2% acetic acid solution for 10 min. Membranes were allowed to dry and were scanned.

Sequencing of DFF45/ICAD$_L$, DFF35/ICAD$_S$, and DFF40/CAD from LN-18 Cells—mRNA was isolated from untreated LN-18 cells using the RNeasy kit (Qiagen) according to the manufacturer's instructions, employing for the extraction the RLN buffer (50 mM Tris-HCl, pH 8.0, 140 mM NaCl, 1.5 mM $MgCl_2$, 0.5% Igepal CA-630, 1,000 units/ml RNase inhibitor, 1 mM DTT). Two micrograms of RNA was reverse-transcribed (Transcriptor First Strand cDNA Synthesis kit; Roche Applied Science) using 10 pmol of random hexamer primer or the specific downstream primer (CAD-R; see below) for 30 min at 65 °C. Two microliters of cDNA was amplified by polymerase chain reaction in an Applied Biosystem thermal cycler 2720 with 300 nM for each primer. The polymerase chain reaction conditions were 95 °C for 20 s, 56 °C for 10 s, and 70 °C for 24 s, repeated 30 cycles in 1.5 mM $MgSO_4$, 200 nM each dNTP, and 1 unit of KOD Hot Start DNA polymerase (Merck). For amplifying DFF40/CAD the following primers were used: CAD-F, 5′-CAGAGGGCTTGAGGACAT-3′ and CAD-R, 5′-TCAGG-

CCTCAAACAAAGACCAGGA-3′. The 1,017-base pair amplified cDNA was automatically sequenced in both directions in a 3130XL genetic analyzer (Applied Biosystems) corresponding to the whole ORF of human DFF40/CAD (GenBank™ accession number NM_004402). For amplifying DFF45/ICAD$_L$ the following primers were used: EcoRI-ICAD-F, 5′-GGAATTCG-GTCCCACCTTGTGGAGGAT-3′ and EcoRI-ICAD-R, 5′-GGAATTCGAGGCTGAGGGTGTCTACCA-3′. The 996-base pair cDNA obtained, corresponding to the whole ORF of human DFF45/ICAD$_L$ (GenBank™ accession number NM_004401), was also sequenced in both directions. Finally, for amplifying DFF35/ICAD$_S$ the following primers were used: EcoRI-ICAD-F, 5′-TGAATTCCACCTCTGCATGATACTA-CTACATCC-3′ and EcoRI-ICAD$_S$-R 5′-CCGCTCGAGCAG-GGCATGTCCTCCTCTGTAG-3′. The 807-base pair cDNA obtained, corresponding to the whole ORF of human DFF35/ICAD$_S$ (GenBank™ accession number NM_213566), was also sequenced in both directions.

Cell-free System to Detect DNA Degradation—Cytoplasms and nuclei from LN-18 and SH-SY5Y cells were prepared as established previously in our laboratory (23). Each reaction was carried out employing 150 μg of cytosolic extract and 10^5 nuclei and stopped by adding 5 mM EDTA after 2 h. Then, reactions were centrifuged for 15 min at 16,000 × *g*, at 4 °C. Supernatants were collected and DNA extracted to discard the LMW DNA fragments as potential contaminant from staurosporine-pretreated SH-SY5Y cytoplasms. The pelleted nuclei were washed once with cytosolic extraction buffer (20 mM Tris-HCl, pH 7.4, 10 mM KCl, 2 mM $MgCl_2$, 1 mM DTT, 0.5 mM EGTA, 2.5% glycerol, 0.5% Igepal CA-630) obtaining the "nuclei wash" fraction that was also DNA-extracted to further ascertain both the absence of DNA after nuclei wash and the purity of the pelleted nuclei. Finally, pelleted nuclei were resuspended in bi-distilled water and processed according to the oligonucleosomal DNA degradation analysis procedure.

Transfection of DFF40/CAD—LN-18 cells were transfected with the eukaryotic expression vector pcDNA3.1 containing or not the open reading frame of the human CAD by using Lipofectamine 2000 Reagent and according to manufacturer's protocol. Transient transfection was analyzed 24 h after transfection. To obtain stably transfected cells, 24 h after transfection, cells were grown in selective medium containing 1 mg/ml G-418 (Geneticin) (Invitrogen) for 25–30 days (until non-transfected cells died in selective medium) and used as a pool.

Cell-free System to Analyze Nuclear Morphology—To obtain isolated nuclei, SH-SY5Y or LN-18 cells were cultured into 6- × 100-mm culture dishes. After confluence, cells were collected and centrifuged at 500 × *g* for 5 min. Pelleted cells were rinsed once with PBS and resuspended in 5 volumes of cell-free extraction buffer (20 mM Hepes-KOH, pH 7.5, 10 mM KCl, 1.5 mM $MgCl_2$, 1 mM DTT) supplemented with 0.2% (for SH-SY5Y cells) or 0.4% (for LN-18 cells) Igepal CA-630. The resuspended cells were kept on ice for 30 min before passing through a 22-gauge syringe (20 times for SH-SY5Y cells or 30 times for LN-18 cells). Then, nuclei were pelleted at 8,000 × *g* for 10 min, resuspended in 700 μl of cell-free extraction buffer containing 0.5 M sacarose and carefully layered on the top of 700 μl of cell-free extraction buffer containing 1.5 M sacarose. After centrifugation at 8,000 × *g* for 10 min, the supernatants were discarded, and pelleted nuclei were washed once with cell-free extraction buffer. Purified nuclei were first resuspended in 2× nuclear storage buffer (20 mM Pipes, pH 7.5, 160 mM KCl, 40 mM NaCl, 10 mM EGTA, 2 mM DTT, 0.5 M sacarose), and finally, the same volume of glycerol was added. Aliquots of 5×10^7 nuclei/ml were prepared and stored at −80 °C until use. To obtain cytosolic extracts, SH-SY5Y or LN-18 cells were treated with 1 μM STP for 24 h or left untreated. Cells were collected and centrifuged at 500 × *g* for 5 min, rinsed once with PBS, and resuspended in 4 volumes of cell-free extraction buffer supplemented with 1 mM PMSF. After 15 min on ice, SH-SY5Y and LN-18 lysates were passed through a 22-gauge syringe 20 or 30 times, respectively. The obtained lysates were purified by means of serial centrifugations at 3,000 × *g* for 5 min, 16,000 × *g* for 5 min, and 100,000 × *g* for 1 h. Finally, aliquots of 100 μg of protein were prepared and stored at −80 °C until use. To perform the cell-free assay, 6×10^5 isolated nuclei and 100 μg of RNA-free cytoplasms (obtained after incubation with 100 ng of RNase at room temperature for 10 min) were employed for each reaction. Each cell-free *in vitro* assay was carried out under mild agitation (350 rpm) at 35 °C in a buffer containing 25 mM Pipes, pH 7.5, 150 mM KCl, 5 mM $MgCl_2$, 1 mM DTT supplemented with an ATP regeneration system (40 μM ATP, 200 μM phophocreatine, 1 μg/ml creatine phosphokinase). The final volume of each reaction was adjusted to 143 μl with cell-free extraction buffer. After the indicated times, the reactions were stopped by adding 1% paraformaldehyde. Nuclei were stained with 0.5 μg/ml Hoechst 33258 and visualized under UV illumination with epifluorescence optics. Representative images of each condition were obtained as aforementioned.

RESULTS

LN-18 Cells Do Not Display Apoptotic Nuclear Features after Staurosporine Treatment—We have previously addressed the molecular and biochemical mechanisms that govern the final steps during cell death by analyzing the nuclear outcomes in different tumor-derived cells exposed to apoptotic insults. Indeed, we have described two main cellular caspase-dependent responses to staurosporine treatment, a broad kinase inhibitor and a well known apoptotic inductor. First, the alkaloid induced a canonical apoptotic response when added to the culture medium of SH-SY5Y cells, including oligonucleosomal DNA degradation and stage II nuclear morphology. However, IMR-5 cells did not display internucleosomal DNA cleavage or stage II nuclear morphology after apoptotic injury (18). Here, we report a new cellular paradigm of apoptotic cell death depicted by the glioblastoma multiforme-derived LN-18 cells. After staurosporine treatment, SH-SY5Y, IMR-5, and LN-18 cells showed comparable percentages of cell death, reaching 86.80%, 92.04%, and 81.95% of trypan blue-positive cells, respectively (Fig. 1*A*, *left*). However, the nuclear aspect displayed by these cells was dissimilar. As expected, and after staurosporine treatment, SH-SY5Y cells underwent stage II nuclear morphology, and IMR-5 cells displayed stage I nuclear morphology (Fig. 1*B*, and *A*, *right*). Nevertheless, LN-18 cells showed a prominent nuclear pyknosis without karyorrhexis (Fig. 1*B*, and *A right*), compatible with stage III nuclear mor-

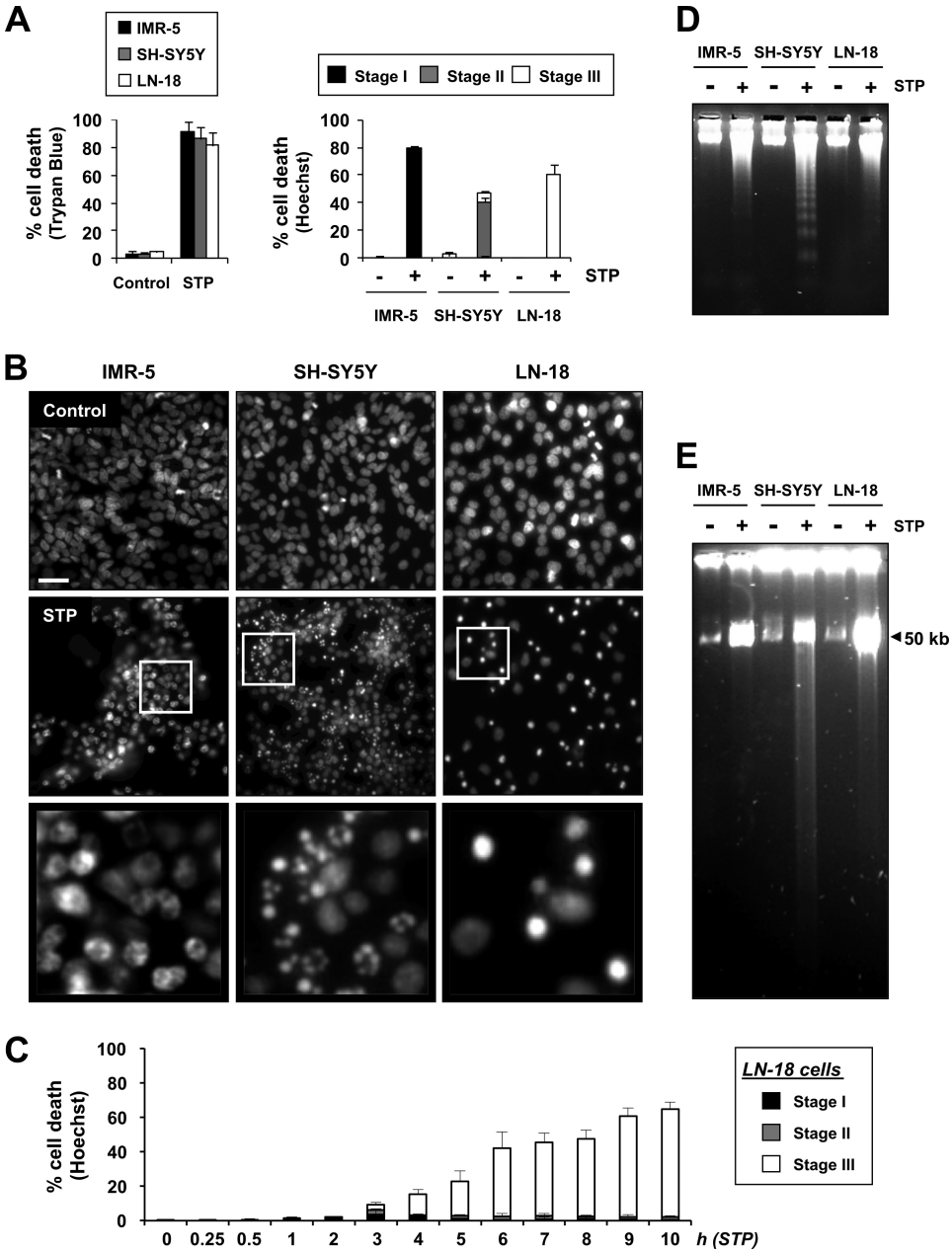

FIGURE 1. **LN-18 cells do not display apoptotic hallmarks during staurosporine-triggered cell death.** IMR-5, LN-18, and SH-SY5Y cells were seeded as described under "Experimental Procedures" and treated with 1 μM staurosporine (*STP* or +) or left untreated (*Control* or −). *A,* cell death was measured by trypan blue exclusion assay after cells were treated for 24 h. *Blue* (dead) cells are represented over total (*blue* and *white*) cells. The graphic represents the means ± S.D. (*error bars*) of >300 cells from three independent experiments. *B*, nuclear morphology was assessed by fixing cells and staining nuclei with Hoechst 33258, 24 h after treatment. Representative images of each condition are shown. The *bottom panels* are higher magnifications of the cells framed in the staurosporine-treated conditions. *Scale bar*, 40 μm. *C*, LN-18 cells were treated with 1 μM STP for the indicated times (hours). Then, cells were fixed and stained with Hoechst 33258. Cell death was calculated by counting stage I (peripheral chromatin condensation), stage II (nuclear collapse and disassembly), or stage III (highly compacted chromatin without signs of karyorrhexis) nuclear morphology. The graph represents the means ± S.D. obtained after counting at least 300 cells for each condition ($n = 3$). *D*, conventional agarose-gel electrophoresis of DNA to detect oligonucleosomal DNA fragmentation after 6 h of treatment. *E*, cells were detached after 4 h of treatment, and genomic integrity was assessed according to the HMW DNA fragmentation analysis procedure.

phology (10). This particular outcome was observed at any time during the treatment with staurosporine (Fig. 1*C*), ruling out the possibility that LN-18 cells could display stage I and/or stage II nuclear morphology throughout cell death. The differences in nuclear changes induced by staurosporine were also corroborated by electron microscopy (Fig. 2). In IMR-5 cells (Fig. 2, *top*), staurosporine induced disruption of intracellular structural organization, including mitochondrial swelling and fragmentation of the rough endoplasmic reticulum. Uneven condensed marginal chromatin appeared homogeneously distributed inside the nucleus, forming irregular and interconnected masses of chromatin in a coarse pattern. Although chromatin condensation was the main nuclear change observed, its texture, shape, and distribution pattern differed from the typical apoptotic images found in SH-SY5Y (Fig. 2, *middle*). The nucleus from staurosporine-treated SH-SY5Y cells contained

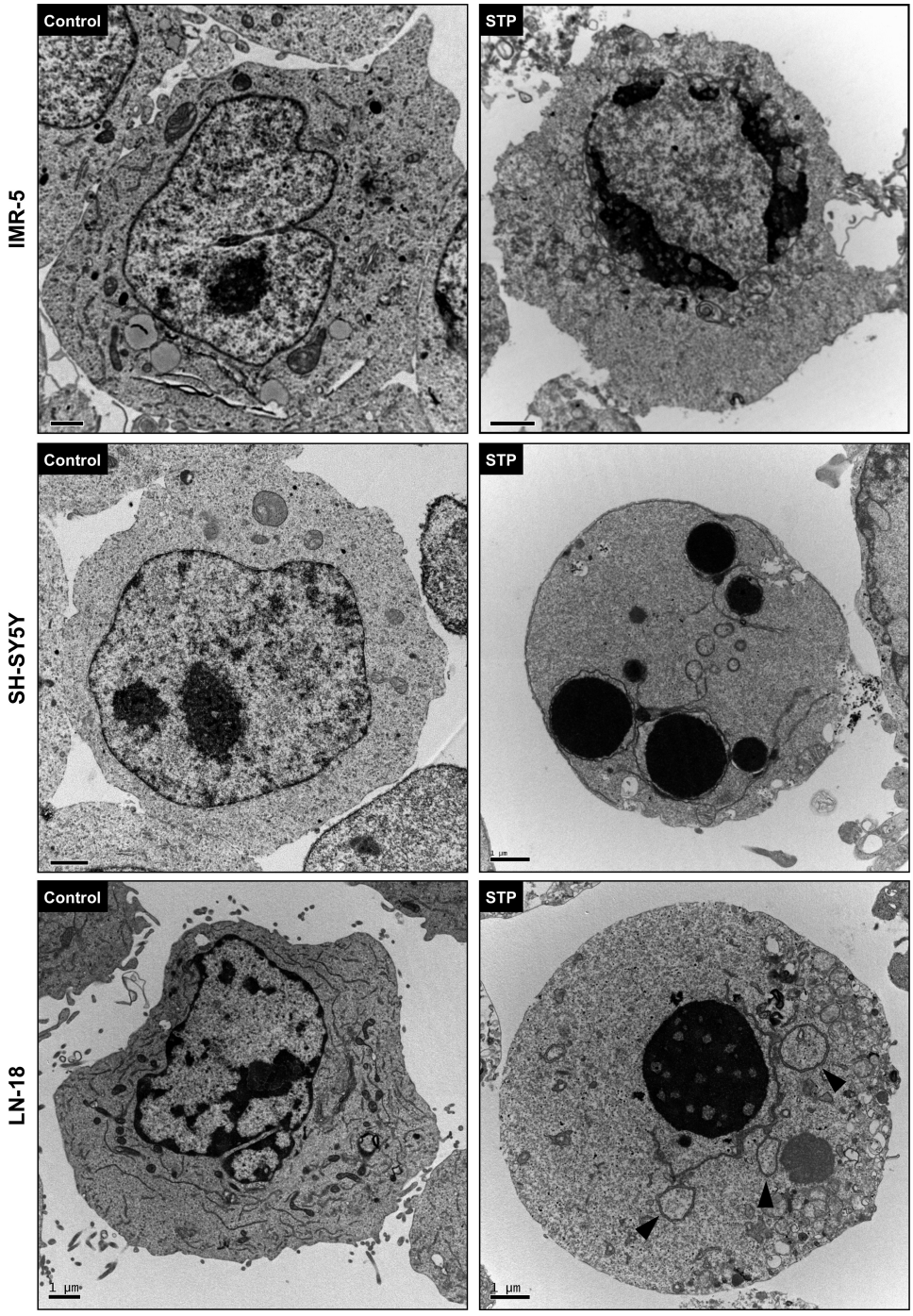

FIGURE 2. **LN-18 cells present nuclear but not chromatin fragmentation after apoptotic stimuli.** Representative images of transmission electron microscopy from IMR-5 (*top*), SH-SY5Y (*middle*), or LN-18 (*bottom*) cells untreated (*left*) or treated with 1 μM STP for 10 h (*right*). *Arrowheads* indicate circular structures from nuclear envelope, empty of packaged chromatin. *Scale bars*, 1 μm.

aggregates of highly condensed granular chromatin distributed beneath the nuclear envelope. The nuclear contour was occasionally misshapen due to protrusions filled with condensed chromatin that eventually split and formed small rounded bodies surrounded by concentric arrangements of membranes that presumably arose from the nuclear envelope. The cytoplasmic matrix appeared highly condensed, and cells adopted smooth contours (Fig. 2, *middle*). In the case of LN-18 cells (Fig. 2, *bottom*), the integrity of the organelles was not preserved after staurosporine treatment. Moreover, the alkaloid provoked the compaction of the nuclear content into a single highly condensed mass of chromatin with electron-lucent areas, albeit the presence of chromatin-free closed loop structures of nuclear envelope compatible with empty apoptotic nuclear bodies (*arrowheads* in Fig. 2, *bottom*). The intracellular components were distributed homogeneously throughout the cell, with no differences between nuclear and cytoplasm content due to the presence of discontinuities in the nuclear envelope. Finally, staurosporine-treated LN-18 cells displayed a moderate accumulation of electron-lucent vacuoles, compatible with lipid

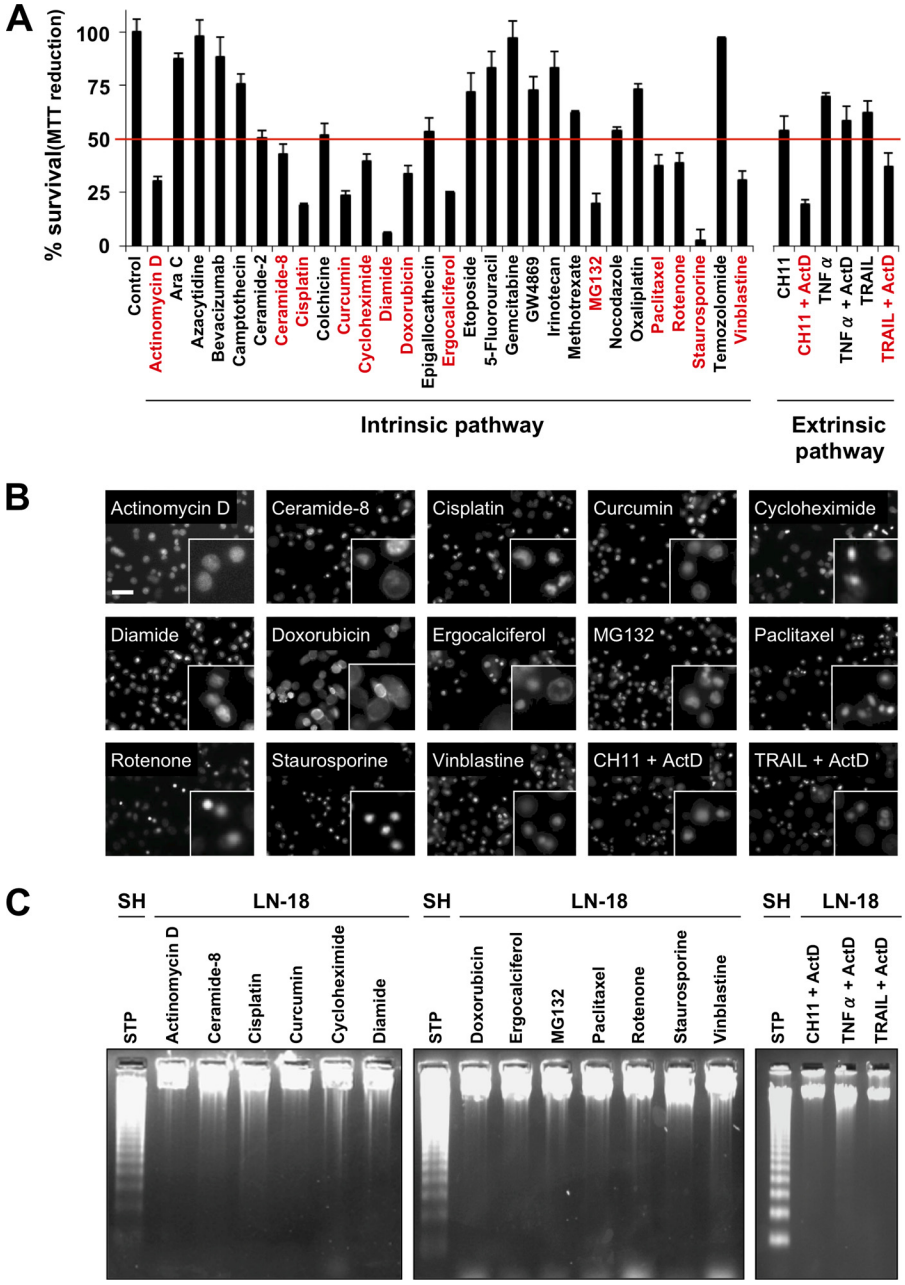

FIGURE 3. **LN-18 cells do not present apoptotic traits after apoptotic stimuli.** LN-18 cells were treated as indicated. *A*, cell viability was measured by MTT reduction assay after 24 h of treatment. Values represent the means ± S.D. (*error bars*; $n = 3$). *B*, nuclear morphology was assessed by fixing cells with paraformaldehyde and staining nuclei with Hoechst 33258 after 24 h of treatment. Representative images are shown. The *insets* framed in the images are higher magnifications of the cells. *Scale bar*, 40 μm. *C*, DNA was extracted 24 h after treatment, and oligonucleosomal DNA degradation was analyzed by convectional agarose gel electrophoresis. DNA from staurosporine-treated SH-SY5Y cells (*SH*) was used as a positive control.

droplets (28). In conclusion, besides subtle cytoplasmic disparities, the most pronounced differences between LN-18 cells and SH-SY5Y or IMR-5 cells were observed at the nuclear level.

LN-18 Cells Display HMW but Not LMW DNA Degradation after Staurosporine Treatment—We have shown previously that SH-SY5Y and IMR-5 cells underwent apoptosis in the presence or the absence, respectively, of oligonucleosome-sized DNA fragments (27). As shown in Fig. 1*D*, staurosporine was able to induce oligonucleosomal DNA degradation in SH-SY5Y cells but not in IMR-5 or LN-18 cells 24 h after treatment. The absence of LMW DNA fragmentation in LN-18 cells was observed in both short (up to 24 h) and long (up to 3 days) treatments (data not shown). However, and as described previously for SH-SY5Y and IMR-5 cells (10), staurosporine-treated LN-18 cells degraded their genomic content into large chromatin fragments, also known as HMW DNA degradation (Fig. 1*E*).

LN-18 Cells Are Defective in Generating the Apoptotic Hallmarks after a Panoply of Cytotoxic Insults—To evaluate whether LN-18 cells can undergo canonical apoptosis, we treated them with a broad battery of apoptotic inductors (see "Experimental Procedures"). First, as extrinsic insults, we used CH-11 (analog of Fas ligand), TNFα, and TRAIL. Second, to switch onto the intrinsic apoptotic pathway we used DNA

TABLE 1
Summary of cell viability, apoptotic nuclear morphology, and DNA laddering in LN-18 cells treated with different chemotherapeutic drugs

Compound	Known mechanism of action	Concentration	% Survival[a] (mean ± S.D.)	Apoptotic nuclei[b]			Ladder[b]
				Stage I	Stage II	Stage III	
1. Actinomycin D (ActD)	Macromolecular synthesis inhibitor	50 μM	30.22 ± 2.02	-	-	-	-
2. Arabinofuranosyl Cytidine (Ara C)	Nucleoside analog	2500 μg/ml	87.51 ± 2.31				
3. Azacytidine	Nucleoside analog	100 μM	97.96 ± 7.54				
4. Bevacizumab	VEGF-A inhibitor	500 μg/ml	88.45 ± 9.01				
5. Camptothecin	Topoisomerase I inhibitor	100 μM	75.70 ± 4.58				
6. Ceramide-2	Not clear, apoptotic inductor	50 μM	50.50 ± 3.48				
7. Ceramide-8	Not clear, apoptotic inductor	50 μM	42.88 ± 4.48	+	-	+	-
8. Cisplatin	DNA cross-linker	50 μg/ml	18.74 ± 0.93	+	-	-	-
9. Colchicine	Microtubule destabilization	50 μM	51.54 ± 5.43				
10. Curcumin	EGFR and NF-kB pathways inhibitor	100 μM	23.53 ± 2.03	+	-	-	-
11. Cycloheximide	Macromolecular synthesis inhibitor	100 μM	39.30 ± 3.76	-	-	+	-
12. Diamide	Thiol oxidating agent	750 μM	5.82 ± 0.30	-	-	-	-
13. Doxorubicin	Topoisomerase I inhibitor	100 μM	33.56 ± 3.87	-	-	-	-
14. Epigallocatechine gallate	Inhibitor of VEGF-mediated tyrosine phosphorylations and Bcl-xL	500 μM	53.59 ± 5.96				
15. Ergocalciferol	Vitamin D2	100 μM	24.67 ± 0.68	+	-	-	-
16. Etoposide	Topoisomerase II inhibitor	100 μM	72.02 ± 8.57				
17. 5-Fluorouracil	Nucleoside analog	1000 μM	83.16 ± 7.57				
18. Gemcitabine	Nucleoside analog	300 μM	97.14 ± 7.76				
19. GW4869	Neutral sphingomyelinase inhibitor	100 μM	72.79 ± 6.17				
20. Irinotecan	Topoisomerase I inhibitor	500 μM	83.29 ± 7.65				
21. Methotrexate	Dihydrofolate reductase inhibitor	500 μM	62.40 ± 4.64				
22. MG132	Proteasome inhibitor	20 μM	19.71 ± 1.54	+	-	-	-
23. Nocodazole	Microtubule destabilization	100 μM	53.80 ± 2.54				
24. Oxaliplatin	DNA cross-linker	100 μg/ml	73.02 ± 5.17				
25. Paclitaxel	Microtubule destabilization	50 μM	37.44 ± 4.53	-	-	+	-
26. Rotenone	Mitochondrial electron transport chain (complex I) inhibitor	100 μM	38.82 ± 5.00	-	-	+	-
27. Staurosporine	Kinase inhibitor	1 μM	2.44 ± 0.30	-	-	+	-
28. Temozolomide	DNA alkylation	50 μM	97.17 ± 4.02				
29. Vinblastine	Microtubule destabilization	25 μM	30.81 ± 5.01	-	-	+	-
30. CH11	Fas ligand analog (apoptotic cytokine)	0.1 μg/ml	53.80 ± 2.17				
31. CH11 + ActD		0.1 μg/ml + 0.04 μM	19.48 ± 1.62	-	-	+	-
32. TNF	Apoptotic cytokine	0.1 μg/ml	69.86 ± 6.77				
33. TNF + ActD		0.1 μg/ml + 0.04 μM	58.46 ± 5.54				
34. TRAIL	Apoptotic cytokine	0.1 μg/ml	62.26 ± 6.30				
35. TRAIL + ActD		0.1 μg/ml + 0.04 μM	36.84 ± 3.91	-	-	+	-

[a] Cell viability was measured by MTT assay after treating cells for 24 h. The values represent the means ± S.D. ($n = 3$). Those under 50% of cell survival are highlighted in red.
[b] When cell viability was lower than 50%, nuclear morphology (scored as stage I (peripheral chromatin condensation), stage II (nuclear collapse and disassembly), or stage III (highly compacted chromatin without signs of karyorrhexis)), and DNA laddering were evaluated. Minus (−) and plus (+) indicate "not detected" and "detected," respectively.

cross-linkers (cisplatin, oxaliplatin), macromolecular synthesis inhibitors (actinomycin D, cycloheximide), microtubule destabilizing agents (colchicine, nocodazole, paclitaxel, vinblastine), topoisomerase inhibitors (camptothecin, doxorubicin, etoposide, irinotecan), nucleoside analogs (5-fluorouracil, cytosine arabinoside, azacytidine, gemcitabine), DNA alkylating agents (temozolomide), oxidizing agents (diamide), among others, such as bevacizumab (inhibitor of VEGF-A), ceramide-2 and -8 (structural components of cell membrane), curcumin (inhibitor of EGFR and NF-κB pathways), ergocalciferol (vitamin D_2), epigallocatechin gallate (inhibitor of VEGF-mediated tyrosine phosphorylations and Bcl-x_L), GW-4869 (inhibitor of neutral sphingomyelinase), methotrexate (dihydrofolate reductase inhibitor), MG132 (inhibitor of proteasome), rotenone (inhibitor of mitochondrial electron transport chain, complex I) and staurosporine. By means of the MTT reduction assays, we obtained different percentages of cell survival after 24 h of treatment (Fig. 3*A* and Table 1). For those drugs that provoked >50% of viability loss, we analyzed the appearance of the nuclei.

According to the nuclear morphology observed, we could classify the drugs employed into four groups: first, chemotherapeutics that mostly induced stage I nuclear morphology (such as cisplatin, curcumin, ergocalciferol, or MG132); second, drugs that induced stage III (including CH-11 or TRAIL, both combined with actinomycin D, cycloheximide, paclitaxel, rotenone, staurosporine, or vinblastine); third, compounds that induced a mixture of stage I and III (ceramide-8); and fourth, actinomycin D, diamide, or doxorubicin, which induced loss of cell viability without major signs of nuclear alterations (Fig. 3*B*, and Table 1). It is worth mentioning that none of the cytotoxic drugs employed was capable of inducing apoptotic stage II nuclear morphology. Accordingly, none of these compounds was able to induce the apoptotic degradation of DNA into oligonucleosome-sized fragments (Fig. 3*C* and Table 1). Taken together, these results demonstrate that LN-18 cells do not display the hallmarks of apoptotic cell death after cytotoxic insult.

LN-18 Cells Undergo Caspase-dependent Cell Death after Staurosporine Treatment—Because DNA laddering and stage II nuclear morphology are the two hallmarks of caspase-dependent apoptosis, we assessed whether LN-18 cells were able to activate caspases after cytotoxic insult. We used staurosporine because our preliminary screenings demonstrated that this alkaloid was the most potent cytotoxic insult. As shown in Fig. 4*A*, the addition of staurosporine to the culture medium induced an increase in DEVD-directed caspase activity, first at 2 h after treatment and reached the highest levels at 6 h. Due to the relevance of executioner caspase-3, -6, and -7 in the cellular dismantling during apoptosis, we wanted to further confirm the correct activation of these three proteases. Using Western blotting, the processing of caspase-3 to its active p17 fragment was observed 4 h after staurosporine treatment (Fig. 4*B*, *first panel*). This processing correlated with the cleavage of α-fodrin to the caspase-3-mediated p120 fragment (Fig. 4*B*, *second panel*), confirming the correct activation of this caspase (29). Likewise, we observed the processing of caspase-6 to its p15 activation fragment 2 h after staurosporine treatment (Fig. 4*B*, *fourth panel*). The fragmentation of lamins A/C, specific substrates of activated caspase-6 (30, 31), to the p51/45 fragments, respectively, corroborated the correct activation of this caspase (Fig. 4*B*, *fifth panel*). Finally, 4 h after staurosporine treatment, we detected caspase-7 processing to its active fragment p20 (Fig. 4*B*, *seventh panel*). The processing of p23 co-chaperone to a p15 fragment, a specific event mediated by active caspase-7 (32),

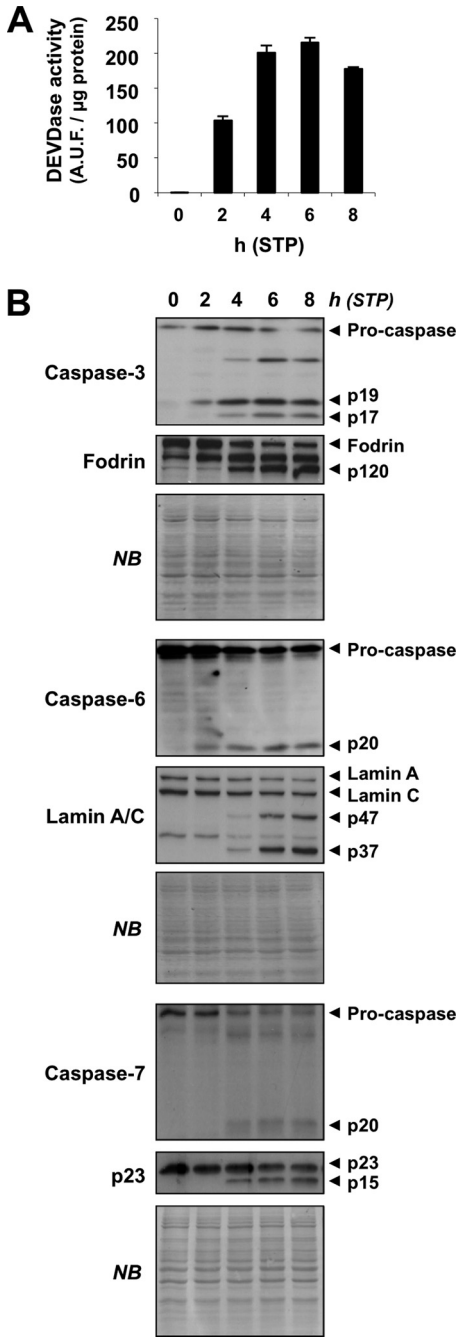

FIGURE 4. **Executioner caspases become correctly activated after staurosporine treatment in LN-18 cells.** LN-18 cells were treated with 1 μM staurosporine for 2, 4, 6, or 8 h, or left untreated (0). After treatment, cells were detached, and proteins extracts were obtained. *A*, DEVD-like activity was measured and graphed. *B*, Western blotting against caspase-3, -6, and -7, and their specific substrates fodrin, lamin A/C, and co-chaperone p23, respectively, were performed. Caspase-3 (p19 and p17), caspase-6 (p20), and caspase-7 (p20) activation fragments are indicated. The activation of caspase-3, -6, or -7 was also corroborated by the detection of p120 (fodrin), p47/p37 (lamin A/C), and p15 (p23 co-chaperone) proteolytic fragments, respectively. Naphthol blue (*NB*) staining served as loading control.

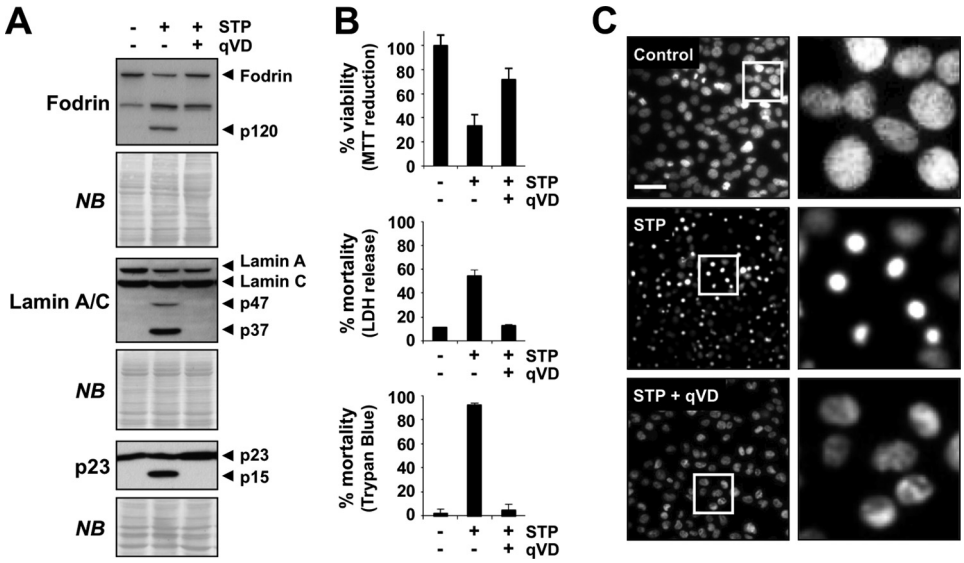

FIGURE 5. **LN-18 cells undergo caspase-dependent cell death upon staurosporine challenge.** LN-18 cells were treated for 24 h with 1 μM STP in the presence (+) or absence (−) of the pan-caspase inhibitor qVD. *A*, proteins extracts were obtained and electrophoresed. Western blotting against fodrin, lamin A/C, and p23 was performed to assess the activation of caspase-3, -6, and -7 by the detection of p120 (fodrin), p47/p37 (lamin A/C), and p15 (p23 co-chaperone) proteolytic fragments, respectively. Naphthol blue (*NB*) served as loading control. *B*, cell viability (measured by MTT reduction assay) and cell death (measured by LDH release or trypan blue exclusion assays) were assessed. Values represent the means ± S.D. (*error bars*) of three independent experiments. *C*, cells were fixed and stained with Hoechst 33258. Representative photographs of each condition (*left*) and the magnification of the *insets* (*right*) are shown. *Scale bar*, 40 μm.

corroborated the correct activation of this protease after staurosporine treatment (Fig. 4*B*, *eighth panel*).

After establishing the correct activation of the executioner caspases-3, -6, and -7 in LN-18 cells, we analyzed their implication in the staurosporine-triggered cell death. To this end, we treated cells for 24 h with staurosporine in the presence or absence of the pan-caspase inhibitor, q-VD-OPh (qVD). After staurosporine treatment, and as explained above, the caspase-mediated cleavages of α-fodrin to p120 fragment, lamin A/C to p47/37 fragments and co-chaperone p23 to p15 fragment were detected by Western blotting indicating the correct activation of executioner caspases-3, -6 and -7, respectively. The presence of qVD completely avoided all these caspase-mediated cleavages (Fig. 5*A*).

Once we demonstrated that qVD prevented the activation of caspases in staurosporine-treated LN-18 cells, we took advantage of this compound to assess the relevance of caspases in triggering cell death. Using the MTT reduction viability assay, we showed that staurosporine-mediated loss of viability was almost completely prevented by qVD (from 33.2 to 71.8%) (Fig. 5*B*, *top panel*). We also analyzed changes in membrane permeability by measuring the extracellular release of LDH. The extracellular LDH activity detected after staurosporine treatment (54.06%) was completely absent when cells were co-treated with qVD (Fig. 5*B*, *middle panel*). Additionally, by using the trypan blue exclusion assay, we confirmed that membrane permeability induced by staurosporine was completely avoided in the presence of the pan-caspase inhibitor (Fig. 5*B*, *bottom panel*). Finally, we analyzed the role of caspases in the nuclear morphology in dead LN-18 cells. The stage III chromatin condensation displayed by cells treated with staurosporine was completely reverted in the presence of qVD (Fig. 5*C*). Taken together, our results showed that both cell death and the nuclear changes observed in staurosporine-treated LN-18 cells depend on caspase activation.

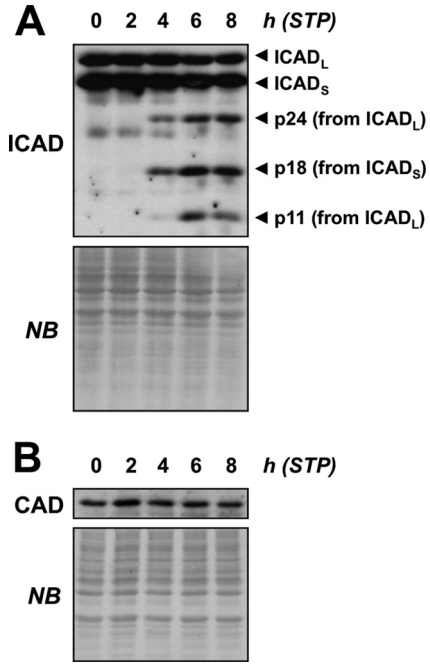

FIGURE 6. **The inhibitor of DFF40/CAD (ICAD) is correctly processed, and DFF40/CAD protein levels remain unaltered throughout staurosporine treatment in LN-18 cells.** LN-18 cells were treated with 1 μM STP for 2, 4, 6, or 8 h or left untreated (0). Then, cells were collected, and proteins were extracted by a buffer containing 1% SDS. Western blots against ICAD (*A*) and CAD (*B*) are shown. The resulting fragments of caspase-3-mediated processing of ICAD are illustrated (p24, p18, and p11). Naphthol blue (*NB*) staining served as loading control.

The Amount of DFF40/CAD Is Not Sufficient to Allow Apoptotic LN-18 Cells to Degrade Their Chromatin into Oligonucleosome-sized Pieces—The activation of the endonuclease DFF40/CAD is the key caspase-mediated event that allows cells to proceed with the final steps of apoptosis (5, 10, 14, 33). Because the executioner caspases were correctly activated in staurosporine-

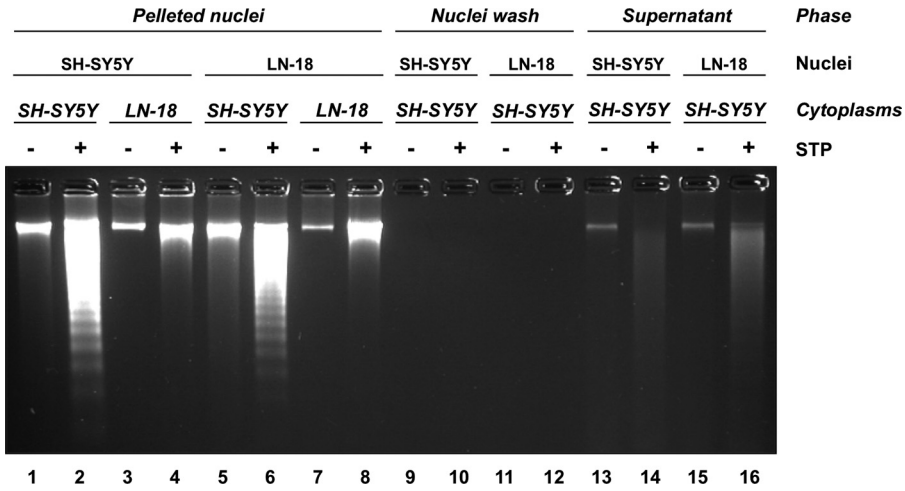

FIGURE 7. **Chromatin of isolated nuclei from LN-18 cells is suitable to be hydrolyzed into oligonucleosome-sized DNA fragments.** *A*, cytoplasms and nuclei from SH-SY5Y or LN-18 cells were obtained as described under "Experimental Procedures." The different fractions were mixed as indicated, and the *in vitro* reactions were performed according to the cell-free system to detect DNA degradation procedure. Then, DNA was extracted from supernatants (*lanes 13–16*), nuclei washes (*lanes 9–12*), or pelleted nuclei (*lanes 1–8*) and electrophoresed to analyze oligonucleosomal DNA fragmentation.

treated LN-18 cells, we studied the activation of DFF40/CAD. To this end, we analyzed the caspase-3-mediated cleavage of ICAD, the inhibitor of DFF40/CAD. We found that the cleavage of ICAD began 4 h after staurosporine treatment (p30 and p24 fragments, from long and short isoforms of ICAD, respectively). After 6 h of treatment, the p11 fragment, corresponding to the C-terminal fragment of $ICAD_L$ was also evidenced (Fig. 6*A*). Moreover, DFF40/CAD was present well over the time of treatment with staurosporine (Fig. 6*B*), excluding the possibility that the defect of LN-18 cells in undergoing canonical apoptosis was due to degradation of the endonuclease (34). To rule out the possibility of a potential mutation in *dff40/cad* or *icad* genes of LN-18 cells affecting the pro-apoptotic function of the endonuclease, the corresponding ORFs were amplified, and the cDNAs obtained were sequenced in both directions. The results obtained revealed wild-type sequences compared with the human DFF40/CAD, $ICAD_L$, and $ICAD_S$ nucleotide consensus sequences from the NCBI nucleotide database (NM_004402, NM_004401, and NM_213566, respectively) (data not shown).

At this point, we asked whether the refractoriness of LN-18 cells to display the hallmarks of apoptosis could be due to the chromatin structure, impairing the endonuclease accessibility to the internucleosomal sites (22). To answer this question, we performed a cell-free assay by isolating nuclei and cytosolic protein extracts from LN-18 or SH-SY5Y cells, SH-SY5Y cells being a positive control that displays DNA laddering (27). As shown in Fig. 7, DNA from LN-18 isolated nuclei incubated with cytoplasms obtained from staurosporine-treated SH-SY5Y cells was degraded into oligonucleosome-sized pieces (*lane 6*). As expected, cytoplasms from staurosporine-treated LN-18 cells did not provoke DNA laddering on LN-18 isolated nuclei (*lane 8*). On the other hand, only cytoplasms from staurosporine-treated SH-SY5Y (*lane 2),* but not those pertaining to LN-18 (*lane 4*) cells, were suitable to induce DNA laddering on SH-SY5Y isolated nuclei. The absence of DNA laddering in both supernatants (*lanes 13–16*) and nuclei washes (*lanes 9–12*) (see "Experimental Procedures") corroborated that the DNA degradation observed in *lanes 1* and 6 was actually generated on the chromatin from isolated nuclei during the *in vitro* reaction. Therefore, the absence of DNA laddering in LN-18 cells is due to an alteration in the apoptotic signaling at the cytosolic level rather than to an intrinsic defect in their chromatin.

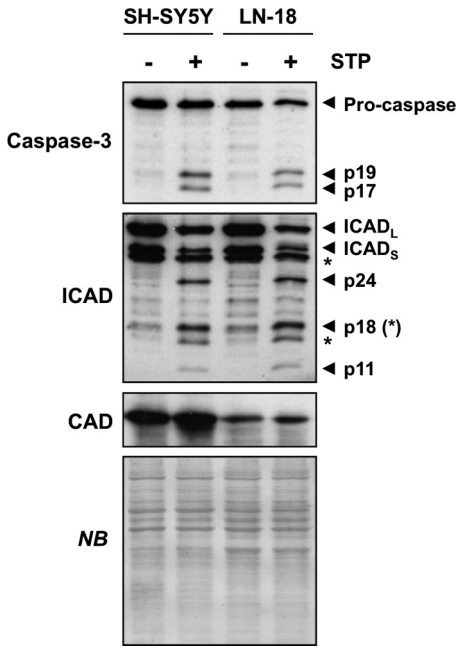

FIGURE 8. **LN-18 cells express lower amount of DFF40/CAD protein compared with SH-SY5Y cells.** SH-SY5Y and LN-18 cells were seeded and treated with 1 μM staurosporine (+) or left untreated (−) for 24 h. The cells were then detached, and total protein extracts were obtained. Western blotting against caspase-3, ICAD, and CAD was performed. Caspase-3 activation and ICAD processing were corroborated by the detection of p19/p17 and p24/p18/p11 fragments, respectively. Note that the bands in the ICAD immunoblot marked with (*) are from the previous immunoblot against caspase-3. Naphthol blue (*NB*) staining served as loading control.

The processing of ICAD by caspase-3, which allows the release and activation of cytosolic DFF40/CAD, is the main molecular event that triggers the oligonucleosomal DNA degradation during apoptosis (23). Therefore, we wanted to compare caspase-3 activation and ICAD processing between LN-18

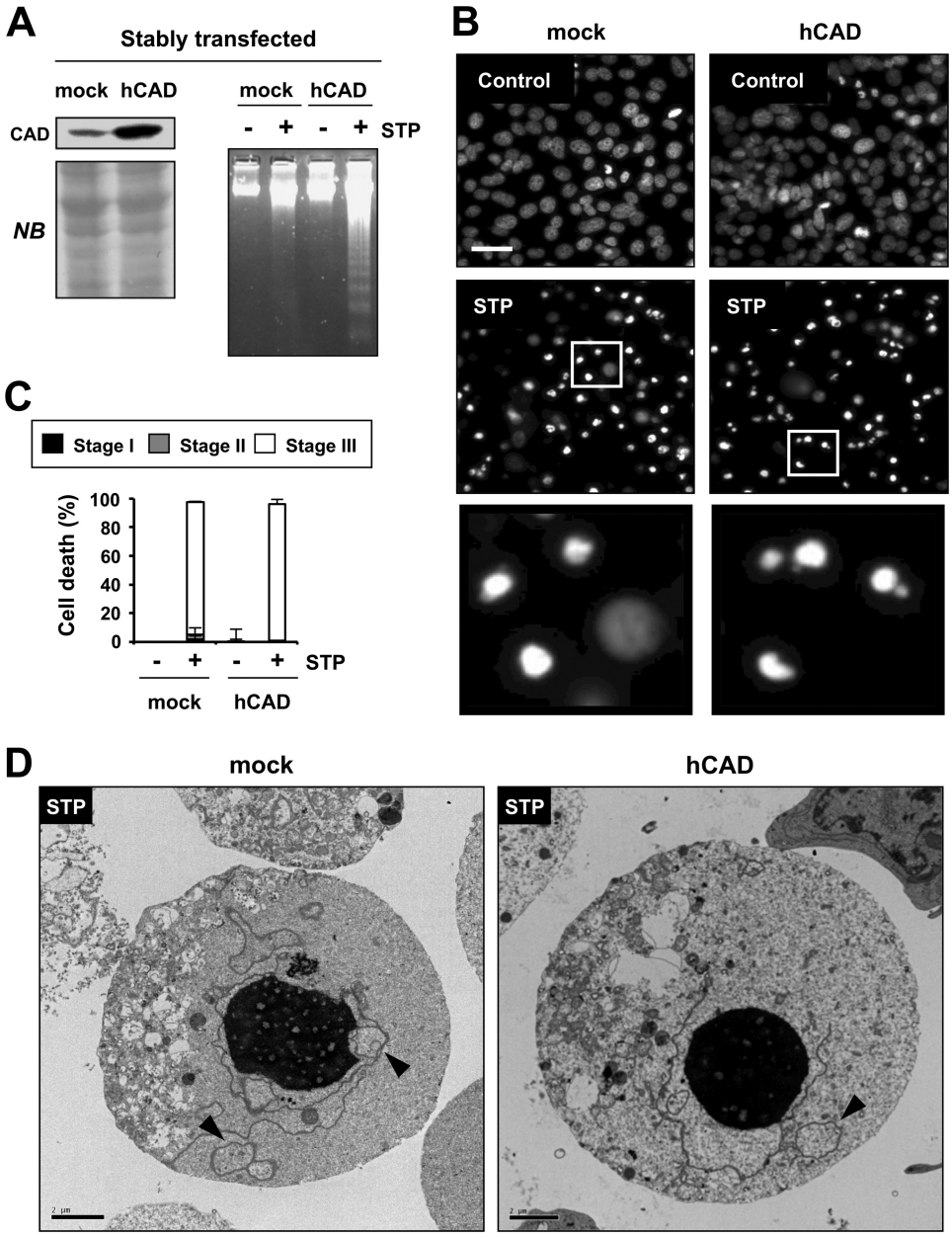

FIGURE 9. **The overexpression of DFF40/CAD does not enable LN-18 cells to display stage II apoptotic nuclear morphology despite triggering oligonucleosomal DNA fragmentation after cytotoxic insult.** *A–D*, LN-18 cells stably transfected with the human ORF of CAD (*hCAD*) or with the empty vector (*mock*) were treated with 1 μM staurosporine (*STP* or +) or left untreated (*Control* or −). *A left*, protein was extracted from untreated cells, and Western blotting against CAD was performed to corroborate the overexpression of the endonuclease. Naphthol blue (*NB*) staining served as loading control. *A right*, DNA from staurosporine-treated (6 h) or untreated cells was obtained and processed according to the LMW DNA degradation analysis protocol. *B*, cells treated (24 h) or left untreated were fixed and stained with Hoechst 33258. Representative microphotographs of each condition are shown. The *right panels* are higher magnifications of the cells framed in the *middle panels*. *Scale bar*, 40 μm. *C*, the percentage of cell death in staurosporine-treated or untreated cells was calculated by counting stage I, stage II, or stage III nuclear morphology. The graph represents the means ± S.D. (*error bars*) obtained after counting >300 cells in each condition ($n = 3$). *D*, representative electron microscopy images from cells treated with staurosporine for 10 h. *Scale bars*, 2 μm. *E*, LN-18 cells stably transfected with hCAD were treated as indicated for 24 h. The cells were then fixed and stained with Hoechst 33258. Representative microphotographs of each condition are shown. The *insets* framed in the images are higher magnifications of the cells. *Scale bar*, 40 μm. *F*, table summarizes cell viability and the stage of apoptotic nuclear morphology observed in CAD-overexpressing LN-18 cells treated with different chemotherapy drugs for 24 h. Cell viability, measured by MTT assay, is represented as the means ± S.D. ($n = 3$). Nuclear morphology was scored as stage I (peripheral chromatin condensation), stage II (nuclear collapse and disassembly), or stage III (highly compacted chromatin without signs of karyorrhexis. Minus (−) and plus (+) indicate "not detected" and "detected," respectively.

and SH-SY5Y cells after staurosporine challenge. As shown in Fig. 8, the alkaloid induced comparable levels of both cleaved caspase-3 and processed ICAD in LN-18 and SH-SY5Y cells. However, the total protein levels of DFF40/CAD were dissimilar, being lower in LN-18 cells, consistent with a DFF40/CAD-deficient constitutive expression in LN-18 cells *versus* SH-5Y5Y cells.

The Overexpression of hCAD Does Not Enable LN-18 Cells to Display Stage II Apoptotic Nuclear Morphology after Cytotoxic Insult Despite Triggering Internucleosomal DNA Fragmentation—Taking into account the results obtained, we stably transfected LN-18 cells with the eukaryotic expression plasmid pcDNA3 carrying the ORF of human CAD (hCAD) or with the

E

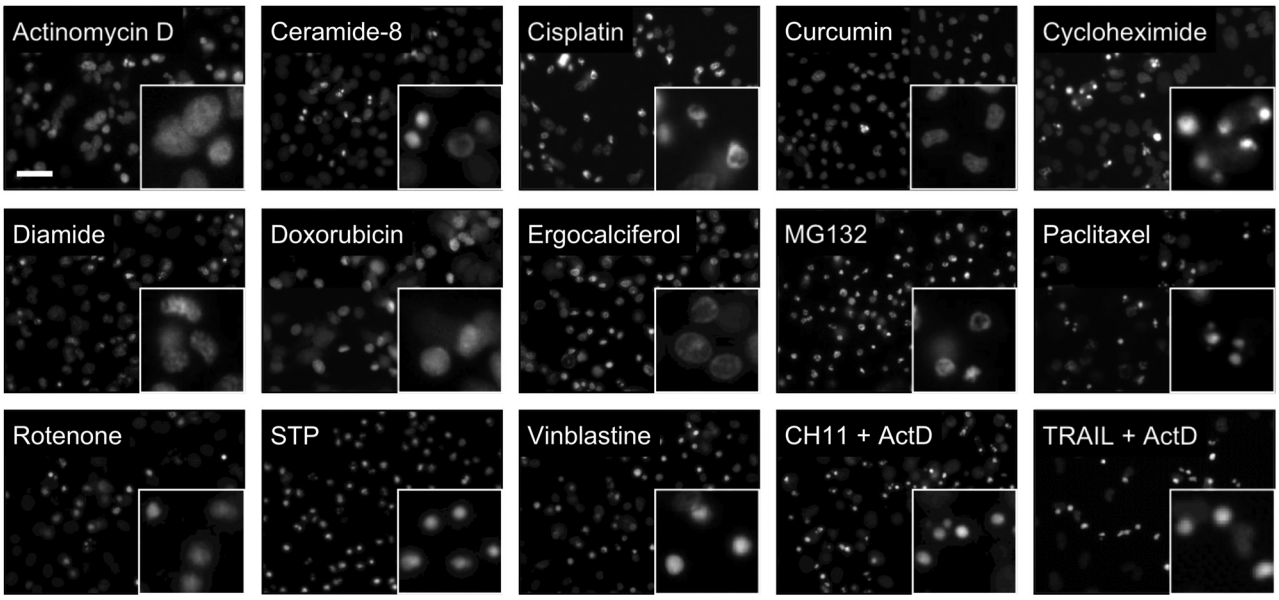

F

Compound	Concentration	% Survival (MTT) (mean ± S.D.)	Apoptotic nuclei		
			Stage I	Stage II	Stage III
1. Actinomycin D (ActD)	50 μM	22.05 ± 1.96	-	-	-
2. Ceramide-8	50 μM	61.87 ± 6.19	+	-	+
3. Cisplatin	50 μg/ml	23.04 ± 1.71	+	-	-
4. Curcumin	100 μM	13.33 ± 1.04	+	-	-
5. Cycloheximide	100 μM	36.46 ± 2.82	-	-	+
6. Diamide	750 μM	5.14 ± 2.51	-	-	-
7. Doxorubicin	100 μM	35.53 ± 1.48	-	-	-
8. Ergocalciferol	100 μM	43.81 ± 5.34	+	-	-
9. MG132	20 μM	20.27 ± 1.67	+	-	-
10. Paclitaxel	50 μM	27.57 ± 1.93	-	-	+
11. Rotenone	100 μM	55.47 ± 4.48	-	-	+
12. Staurosporine	1 μM	4.97 ± 0.55	-	-	+
13. Vinblastine	25 μM	38.07 ± 2.12	-	-	+
14. CH11 + ActD	0.1 μg/ml + 0.04 μM	17.80 ± 1.39	-	-	+
15. TRAIL + ActD	0.1 μg/ml + 0.04 μM	45.30 ± 4.26	-	-	+

FIGURE 9 —*continued*

empty vector (mock). After corroborating the expression levels of DFF40/CAD (Fig. 9*A*, *left panel*), we treated cells with staurosporine for 24 h. We found that CAD-overexpressing, but not mock-transfected, cells displayed internucleosomal DNA cleavage after staurosporine treatment (Fig. 9*A*, *right panel*). The analysis of the nuclei revealed that the transfection with the empty vector did not affect the nuclear morphology observed previously in LN-18-nontransfected cells, including either staurosporine-treated or nontreated cells (Fig. 9*B*). Surprisingly, CAD-overexpressing cells showed highly condensed chromatin without signs of nuclear fragmentation after staurosporine challenge (Fig. 9*B*). In fact, the percentage of cells displaying nuclear pyknosis and karyorrhexis (stage II nuclear morphology) never exceeded 3% of the total cell population (Fig. 9*C*). Ultrastructurally, staurosporine-treated hCAD-overexpressing LN-18 cells presented a unique mass of highly condensed chromatin, containing small electron-lucent areas. The nuclear envelope appeared disrupted, whereas the nuclei remained unfragmented. At the cytoplasmic level, we observed a heterogeneous content with abundant low dense intrusions compatible with lipid droplets (Fig. 9*D*). We obtained the same results by transient transfection of DFF40/CAD, ruling out a

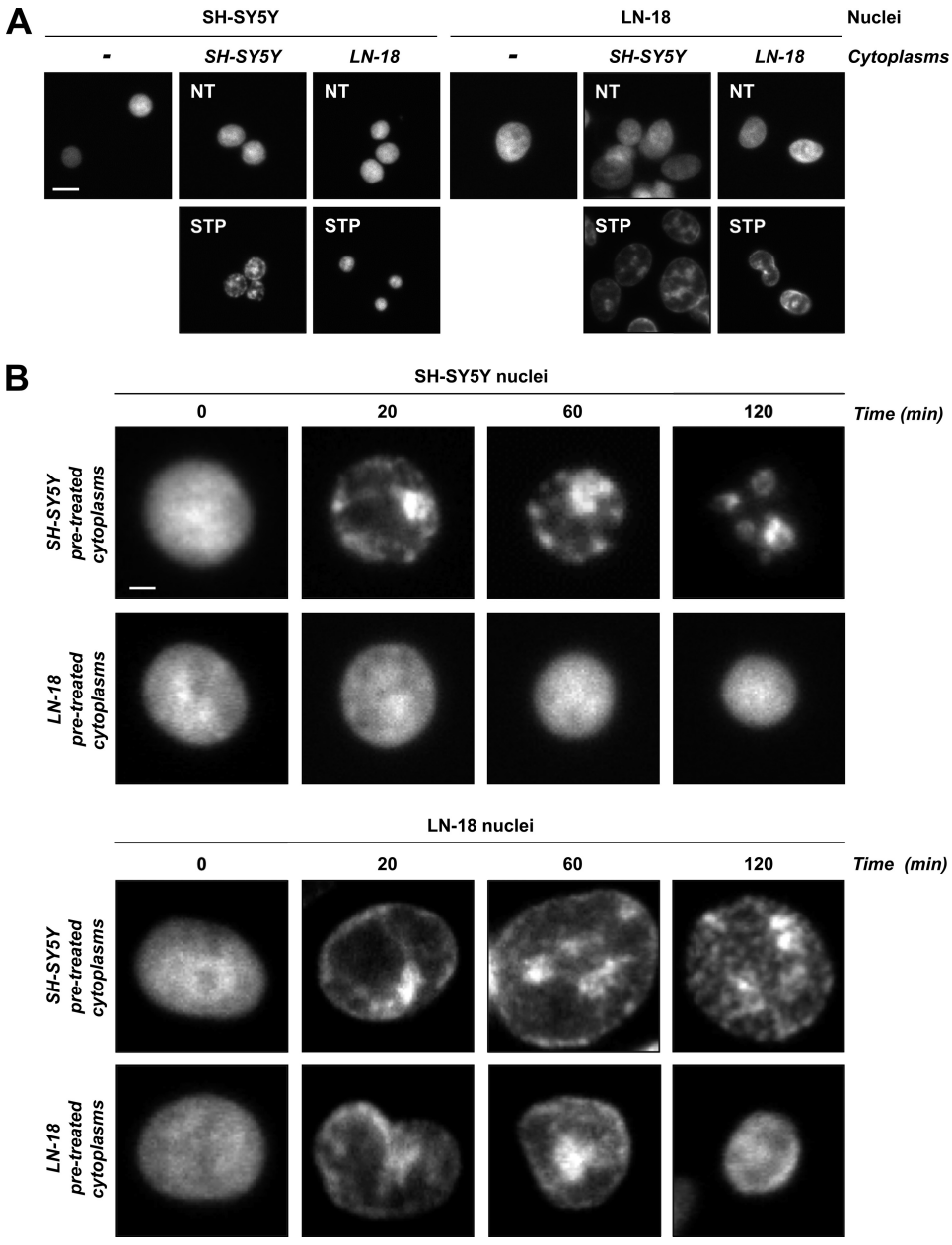

FIGURE 10. **The refractoriness of LN-18 cells to undergo apoptotic nuclear morphology relies on both nuclear and cytoplasmic impairments.** Cytoplasms and nuclei from SH-SY5Y or LN-18 cells were obtained as described under "Experimental Procedures." The different fractions were mixed as indicated, and the *in vitro* reactions were performed according to the cell-free system to analyze nuclear morphology procedure. *A*, after 60 min of *in vitro* reaction, the nuclei were fixed with 1% paraformaldehyde and stained with Hoechst 33258. Representative images of each condition are shown. *Scale bar*, 20 μm. *B*, time course of cell-free reactions is shown. Representative images of cells fixed and stained with Hoechst 33258 were obtained at the indicated times. *Scale bar*, 5 μm.

partial loss of function of the endonuclease over cell culture. (data not shown). We then sought to explore whether CAD overexpression allowed other apoptotic insults to induce stage II nuclear morphology. None of the cytotoxic drugs, which effectively provoked loss of cell viability in both non-transfected (Fig. 3*A* and Table 1) and CAD-overexpressing LN-18 cells (Fig. 9*F*), induced stage II nuclear morphology in CAD-overexpressing cells (Fig. 9, *E* and *F*). Therefore, making LN-18 cells express higher levels of DFF40/CAD is not sufficient to allow apoptotic chromatin fragmentation in cells committed to die.

Isolated Nuclei from LN-18 Cells Remain Unfragmented after Incubation with Apoptotic Cytoplasms in Vitro—So far, our results showed the inability of LN-18 cells to display oligonucleosomal DNA degradation during apoptosis, which can be solved either by DFF40/CAD overexpression or by incubating isolated nuclei with staurosporine-pretreated cytoplasms from SH-SY5Y cells. However, overexpression of the endonuclease was insufficient to generate apoptotic nuclear morphology. Therefore, we decided to establish a cell-free assay to analyze nuclear fragmentation.

The nuclei isolated from SH-SY5Y cells responded differentially to cytoplasms from staurosporine-treated SH-SY5Y or LN-18 cells. When they were incubated with preactivated cytoplasms from SH-SY5Y cells, the chromatin adopted a necklace shape, compatible with an intermediate stage II apoptotic nuclear morphology (35). However, when incubated with cyto-

plasms from staurosporine-treated LN-18 cells, SH-SY5Y nuclei collapsed, showing a chromatin condensation similar to that observed in LN-18 cells *in vivo* (Fig. 10*A*). However, when LN-18 nuclei were employed, the morphological alterations observed were noticeably different from those detected in SH-SY5Y nuclei. When exposed to staurosporine-treated cytoplasms from either SH-SY5Y or LN-18 cells, their chromatin appeared condensed in a continuous ring at the interior surface of the nuclear envelope, compatible with stage I apoptotic nuclear morphology. However, whereas LN-18 nuclei exposed to preactivated cytoplasms from SH-SY5Y cells appeared swollen, those incubated with preactivated cytoplasms from LN-18 cells became visibly wrinkly (Fig. 10*A*). It was noted that after 60 min of *in vitro* reaction, cytoplasms from untreated SH-SY5Y or LN-18 cells did not induce any significant change in either SH-SY5Y or LN-18 isolated nuclei (Fig. 10*A*).

After an incubation period with SH-SY5Y pre-treated cytoplasms, SH-SY5Y nuclei showed different apoptotic stages: first, small masses of condensed chromatin at 20 min, followed by a necklace appearance at 60 min, and finally, the fragmentation of the nucleus after 2 h of *in vitro* assay (Fig. 10*B*). When LN-18 preactivated cytoplasms were used, SH-SY5Y nuclei progressively shrank, acquiring an aspect resembling the aforementioned stage III apoptotic nuclear morphology. However, LN-18 nuclei underwent a progressive swelling in the presence of preactivated cytoplasms from SH-SY5Y cells. The chromatin, although peripherally distributed at the beginning of the assay (20 and 60 min), appeared microfragmented after 120 min of *in vitro* reaction. Similarly, after 20 and 60 min of assay, LN-18 nuclei mixed with preactivated LN-18 cytoplasms displayed peripherally condensed chromatin. However, under these conditions, LN-18 nuclei suffered a gradual shrinkage which, after 120 min of reaction, resembled that observed in SH-SY5Y isolated nuclei after 60 or 120 min of incubation with LN-18 preactivated cytoplasms (Fig. 10*B*). Altogether, LN-18 cells appear to be equipped with molecular cues to reject completion of apoptosis. They are localized both in the cytoplasm and in the nucleus and prevent the preactivated cytoplasm from promoting the formation of chromatin clumps and support nuclear chromatin refractoriness to be fragmented.

DISCUSSION

We now describe a new apoptotic behavior depicted by LN-18 cells, a human glioblastoma-derived cell line. After apoptotic insult, LN-18 cells undergo abortive caspase-dependent apoptosis in which neither chromatin disassembly nor oligonucleosomal DNA breakdown takes place despite cell death. The amount of DFF40/CAD is the key event explaining the refractoriness of LN-18 cells to degrade their genomic content into oligonucleosome-sized fragments. Indeed, the overexpression of this endonuclease is sufficient to enable LN-18 cells to generate DNA laddering after staurosporine treatment. Intriguingly, the overexpression of this endonuclease does not affect the nuclear changes observed in wild-type cells after cytotoxic insult. Moreover, using cell-free *in vitro* assays we show that both nuclei and cytoplasm from LN-18 cells behave in an aberrant apoptotic fashion. This is the first report on a cellular model in which DFF40/CAD overexpression makes cells competent for DNA laddering, but does not allow them to undergo stage II nuclear morphology upon apoptotic insult.

Up until now, three different cellular responses have been reported as regard the presence or not of the two apoptotic hallmarks during caspase-dependent cell death: first, cells that display both stage II nuclear morphology and DNA ladder (*e.g.* SH-SY5Y and NB69 cells, among others) (18); second, cells displaying none of these apoptotic hallmarks (*e.g.* IMR-5, IMR-32, and LAI-5S cells) (18, 23, 27); and third, cells showing stage II nuclear morphology but not oligonucleosomal DNA breakdown (*e.g.* MOLT-4 and SK-N-AS cells) (21, 23). In all cases, cells need functional DFF40/CAD to display both hallmarks after caspase activation. Indeed, DFF40/CAD knockdown avoids stage II nuclear morphology (revealing stage I nuclear morphology) and oligonucleosomal DNA degradation in cells proficient to display any of the apoptotic hallmarks (33). In the same sense, the overexpression of this endonuclease is enough to facilitate the apoptotic hallmarks in those cells that are defective in displaying them (33). In LN-18 cells, as expected, the overexpression of DFF40/CAD provides the ability to degrade the chromatin into oligonucleosomal length fragments. Interestingly, although caspase-dependent, the nuclear morphology observed in apoptotic LN-18 cells is not affected by DFF40/CAD overexpression or the specific knockdown of this endonuclease.[7]

Nuclear shrinkage and disassembly and oligonucleosomal DNA breakdown during apoptosis were classically considered to arise concomitantly or, at least, be closely related (16–19). The close relationship that exists between both apoptotic hallmarks relied on DFF 40/CAD. In fact, the proper activation of this endonuclease seems the molecular key bottleneck allowing cells to display both apoptotic hallmarks after the proteolytic action of caspases. In neuroblastoma-derived IMR-5 cells, for example, the disappearance of DFF40/CAD during caspase-dependent apoptosis correlates with the absence of both internucleosomal DNA cleavage and stage II nuclear morphology, despite the proper activation of caspase-3 (10, 18, 27). Furthermore, SH-SY5Y cells, a classical cellular model that undergoes canonical apoptotic cell death, fail to display either of the apoptotic hallmarks after their treatment with high cytotoxic concentrations of methadone because of DFF40/CAD proteolysis (34). The latest reports on some cellular models undergoing caspase-dependent cell death, characterized by the presence of stage II nuclear morphology without oligonucleosomal DNA degradation, suggest a dissociation between both processes (20–23). However, DFF40/CAD is still required. In this regard, we have recently reported that the nuclear collapse and disassembly observed during caspase-dependent cell death in SK-N-AS cells, which fail to degrade their DNA into oligonucleosome-sized fragments depend on DFF40/CAD catalytic activity (33). LN-18 cells although undergoing caspase-dependent cell death, are unable to degrade their genomic content into oligonucleosome-sized fragments, irrespectively of the drug employed. As regards the nuclear aspect after bisbenzimide staining, and depending on the cytotoxic insult used, injured LN-18 cells can display either stage I chromatin compaction or stage II-like nuclear condensation, characterized by showing no

[7] M. Sánchez-Osuna and V. J. Yuste, unpublished results.

signs of karyorrhexis. The deficiency of LN-18 cells to show nuclear fragmentation is not due to improper caspase activation because both cell demise and the nuclear changes observed are completely reverted when cells are cultured in the presence of a pan-caspase inhibitor. It is worth noting that the data obtained from LN-18 cells show that chromatin packaging and nuclear disassembly are two processes that can be molecularly dissociated. Interestingly, this particular apoptotic response was also observed in other cell lines, such as U87MG or T98G cells.[7]

The analysis of the apoptotic behavior of LN-18 cells has allowed us to add another molecular clue to the controlling of the nuclear changes during caspase-dependent cell death. In fact, this is the first report on a cellular model in which the compaction of the chromatin is independent of the enzymatic action of DFF40/CAD. Our finding appears to be discordant with previous data establishing that the alteration of DFF40/CAD function abolishes both chromatin compaction and nuclear apoptotic body formation (10, 12, 33, 36, 37). An alternative explanation might be that DFF40/CAD-mediated apoptotic signaling is necessary but not sufficient to induce the complete chromatin reorganization during apoptosis, and other DFF40/CAD-independent intracellular pathways are involved. The packaging of the chromatin during apoptosis is a dynamic process. Besides DFF40/CAD, some other molecules have emerged as additional factors that influence apoptotic nuclear packaging (38). Acinus, upon caspase-3 cleavage, induces chromatin condensation in a cell-free system (39). Conversely, the knockdown of acinus does not impede chromatin packaging during apoptotic cell death (40). Thus, the role of this molecule in apoptotic nuclear shrinkage is still unclear. The actin dynamics is another factor influencing cell shape and nuclear changes during apoptosis. Widlak and colleagues have shown that inhibitors of actin depolymerization reduce chromatin condensation, but not DNA fragmentation, in cultured cells undergoing apoptosis (41). In another work, Wakabayashi and collaborators showed that physicochemical states of actin play a role in the execution phase of apoptotic processes (42). Indeed, the addition of jasplakinolide, a stabilizer of F-actin, or latrunculin A, a destabilizer of F-actin, to the culture medium of injured cells, prevents cell fragmentation, nuclear pyknosis, and karyorrhexis (42). However, the alteration of actin dynamics does not allow distinguishing between apoptotic chromatin package and nuclear fragmentation processes. Indeed, there are no data so far reported on whether DNA compaction and nuclear disassembly can occur separately, and it is considered that they both arise concomitantly during the last stage of nuclear changes (35). Here, we have identified LN-18 cells, which undergo distinctive nuclear changes during caspase-dependent cell death. The microscopic aspect of bisbenzimide-stained nuclei from LN-18 cells treated with different apoptotic agents shows that the genomic content becomes compacted in a unique mass, without chromatin clumps of smaller size. However, the ultrastructural analysis of staurosporine-treated LN-18 cells reveals the presence of chromatin-free intracellular bodies, surrounded by a double membrane, which are compatible with the buds observed during apoptotic nuclear fragmentation (43). The presence of such condensed chromatin-free structures in injured LN-18 cells suggests the existence of an unknown mechanism regulating the maintenance of the packaged chromatin in nuclear apoptotic bodies. Interestingly, the presence of condensed chromatin inside the nuclear buds is independent of double-strand oligonucleosomal DNA fragmentation because vDFF40/CAD-overexpressing LN-18 cells are still unable to undergo stage II nuclear morphology after apoptotic insult. Thus, the molecular mechanisms governing the deposition of the packaged chromatin into the apoptotic nuclear bodies are more intricate than initially expected. Moreover, although closely interconnected, the molecular players controlling apoptotic chromatin fragmentation, compaction and deposition into nuclear apoptotic bodies should be distinct. Supporting this idea, the chromatin of isolated nuclei from LN-18 cells is able to be degraded into oligonucleosomal length DNA pieces by a competent apoptotic cytoplasm and yet unable to become packaged into the apoptotic nuclear bodies.

In summary, the DFF40/CAD-independent apoptotic phenotype observed in LN-18 cells after cytotoxic insult unveils a novel unexplored avenue for caspase-dependent cell death. The consequences of the so far untested cell death paradigm are of biological significance, given the relevance of correct cell dismantling in avoiding undesirable pathophysiological effects. Indeed, the phenotypic aspect of an apoptotic cell has been of special interest because defective or abortive apoptosis represents a major causative factor in the development and progression of cancer (44, 45). A correct genomic content packaging of a cell committed to die would minimize the spreading of harmful genes, such as oncogenes or viral DNA. In this context, extracellular DNA from dead cells can activate intracellular pathways in living "receptor" cells, leading to disparate consequences that range from cytotoxicity to cellular transformation (46, 47). Therefore, knowing how chromatin collapse and nuclear disassembly are regulated during caspase-dependent apoptosis could be instrumental for understanding the intimate mechanism that governs an accurate and silent non-harmful cell death. Hence, LN-18 cells are a valuable tool to dissect the biochemical mechanisms that stepwise govern apoptotic chromatin compaction and its final deposition into the apoptotic nuclear bodies.

Acknowledgments—We thank the Personnel of Servei de Microscopia and Servei de Genòmica i Bioinformàtica, Universitat Autònoma de Barcelona; all other members of the laboratory for helpful criticisms; Laura Martínez-Escardó and Ricard Canals-Florit for contribution to the sequencing of ICAD isoforms; and to Dr. Rafaela Cañete-Soler for reading the manuscript.

REFERENCES

1. Lecoeur, H. (2002) Nuclear apoptosis detection by flow cytometry: influence of endogenous endonucleases. *Exp. Cell Res.* **277,** 1–14
2. Susin, S. A., Daugas, E., Ravagnan, L., Samejima, K., Zamzami, N., Loeffler, M., Costantini, P., Ferri, K. F., Irinopoulou, T., Prévost, M. C., Brothers, G., Mak, T. W., Penninger, J., Earnshaw, W. C., and Kroemer, G. (2000) Two distinct pathways leading to nuclear apoptosis. *J. Exp. Med.* **192,** 571–580
3. Wyllie, A. H., Morris, R. G., Smith, A. L., and Dunlop, D. (1984) Chromatin cleavage in apoptosis: association with condensed chromatin morphology and dependence on macromolecular synthesis. *J. Pathol.* **142,** 67–77
4. Zamzami, N., and Kroemer, G. (1999) Condensed matter in cell death.

Nature **401,** 127–128
5. Liu, X., Zou, H., Slaughter, C., and Wang, X. (1997) DFF, a heterodimeric protein that functions downstream of caspase-3 to trigger DNA fragmentation during apoptosis. *Cell* **89,** 175–184
6. Walker, P. R., and Sikorska, M. (1997) New aspects of the mechanism of DNA fragmentation in apoptosis. *Biochem. Cell Biol.* **75,** 287–299
7. Riedl, S. J., and Shi, Y. (2004) Molecular mechanisms of caspase regulation during apoptosis. *Nat. Rev. Mol. Cell Biol.* **5,** 897–907
8. Pop, C., and Salvesen, G. S. (2009) Human caspases: activation, specificity, and regulation. *J. Biol. Chem.* **284,** 21777–21781
9. Elmore, S. (2007) Apoptosis: a review of programmed cell death. *Toxicol. Pathol.* **35,** 495–516
10. Yuste, V. J., Sánchez-López, I., Solé, C., Moubarak, R. S., Bayascas, J. R., Dolcet, X., Encinas, M., Susin, S. A., and Comella, J. X. (2005) The contribution of apoptosis-inducing factor, caspase-activated DNase, and inhibitor of caspase-activated DNase to the nuclear phenotype and DNA degradation during apoptosis. *J. Biol. Chem.* **280,** 35670–35683
11. Wlodkowic, D., Telford, W., Skommer, J., and Darzynkiewicz, Z. (2011) Apoptosis and beyond: cytometry in studies of programmed cell death. *Methods Cell Biol.* **103,** 55–98
12. Liu, X., Li, P., Widlak, P., Zou, H., Luo, X., Garrard, W. T., and Wang, X. (1998) The 40-kDa subunit of DNA fragmentation factor induces DNA fragmentation and chromatin condensation during apoptosis. *Proc. Natl. Acad. Sci. U.S.A.* **95,** 8461–8466
13. Halenbeck, R., MacDonald, H., Roulston, A., Chen, T. T., Conroy, L., and Williams, L. T. (1998) CPAN, a human nuclease regulated by the caspase-sensitive inhibitor DFF45. *Curr. Biol.* **8,** 537–540
14. Enari, M., Sakahira, H., Yokoyama, H., Okawa, K., Iwamatsu, A., and Nagata, S. (1998) A caspase-activated DNase that degrades DNA during apoptosis, and its inhibitor ICAD. *Nature* **391,** 43–50
15. Sakahira, H., Enari, M., and Nagata, S. (1998) Cleavage of CAD inhibitor in CAD activation and DNA degradation during apoptosis. *Nature* **391,** 96–99
16. Steller, H. (1995) Mechanisms and genes of cellular suicide. *Science* **267,** 1445–1449
17. Jacobson, M. D., Weil, M., and Raff, M. C. (1997) Programmed cell death in animal development. *Cell* **88,** 347–354
18. Boix, J., Llecha, N., Yuste, V. J., and Comella, J. X. (1997) Characterization of the cell death process induced by staurosporine in human neuroblastoma cell lines. *Neuropharmacology* **36,** 811–821
19. Samejima, K., Tone, S., and Earnshaw, W. C. (2001) CAD/DFF40 nuclease is dispensable for high molecular weight DNA cleavage and stage I chromatin condensation in apoptosis. *J. Biol. Chem.* **276,** 45427–45432
20. Oberhammer, F., Wilson, J. W., Dive, C., Morris, I. D., Hickman, J. A., Wakeling, A. E., Walker, P. R., and Sikorska, M. (1993) Apoptotic death in epithelial cells: cleavage of DNA to 300 and/or 50 kb fragments prior to or in the absence of internucleosomal fragmentation. *EMBO J.* **12,** 3679–3684
21. Falcieri, E., Martelli, A. M., Bareggi, R., Cataldi, A., and Cocco, L. (1993) The protein kinase inhibitor staurosporine induces morphological changes typical of apoptosis in MOLT-4 cells without concomitant DNA fragmentation. *Biochem. Biophys. Res. Commun.* **193,** 19–25
22. Kuribayashi, N., Sakagami, H., Iida, M., and Takeda, M. (1996) Chromatin structure and endonuclease sensitivity in human leukemic cell lines. *Anticancer Res.* **16,** 1225–1230
23. Iglesias-Guimarais, V., Gil-Guiñon, E., Gabernet, G., García-Belinchon, M., Sánchez-Osuna, M., Casanelles, E., Comella, J. X., and Yuste, V. J. (2012) Apoptotic DNA degradation into oligonucleosomal fragments, but not apoptotic nuclear morphology, relies on a cytosolic pool of DFF40/CAD endonuclease. *J. Biol. Chem.* **287,** 7766–7779
24. Gozzelino, R., Sole, C., Llecha, N., Segura, M. F., Moubarak, R. S., Iglesias-Guimarais, V., Perez-Garcia, M. J., Reix, S., Zhang, J., Badiola, N., Sanchis, D., Rodriguez-Alvarez, J., Trullas, R., Yuste, V. J., and Comella, J. X. (2008) BCL-XL regulates TNF-α-mediated cell death independently of NF-κB, FLIP and IAPs. *Cell Res.* **18,** 1020–1036
25. Decker, T., and Lohmann-Matthes, M. L. (1988) A quick and simple method for the quantitation of lactate dehydrogenase release in measurements of cellular cytotoxicity and tumor necrosis factor (TNF) activity. *J. Immunol. Methods* **115,** 61–69
26. Ribas, J., Yuste, V. J., Garrofé-Ochoa, X., Meijer, L., Esquerda, J. E., and Boix, J. (2008) 7-Bromoindirubin-3′-oxime uncovers a serine protease-mediated paradigm of necrotic cell death. *Biochem. Pharmacol.* **76,** 39–52
27. Yuste, V. J., Bayascas, J. R., Llecha, N., Sánchez-López, I., Boix, J., and Comella, J. X. (2001) The absence of oligonucleosomal DNA fragmentation during apoptosis of IMR-5 neuroblastoma cells: disappearance of the caspase-activated DNase. *J. Biol. Chem.* **276,** 22323–22331
28. Boix, J., Fibla, J., Yuste, V., Piulats, J. M., Llecha, N., and Comella, J. X. (1998) Serum deprivation and protein synthesis inhibition induce two different apoptotic processes in N18 neuroblastoma cells. *Exp. Cell Res.* **238,** 422–429
29. Jänicke, R. U., Ng, P., Sprengart, M. L., and Porter, A. G. (1998) Caspase-3 is required for α-fodrin cleavage but dispensable for cleavage of other death substrates in apoptosis. *J. Biol. Chem.* **273,** 15540–15545
30. Orth, K., Chinnaiyan, A. M., Garg, M., Froelich, C. J., and Dixit, V. M. (1996) The CED-3/ICE-like protease Mch2 is activated during apoptosis and cleaves the death substrate lamin A. *J. Biol. Chem.* **271,** 16443–16446
31. Takahashi, A., Alnemri, E. S., Lazebnik, Y. A., Fernandes-Alnemri, T., Litwack, G., Moir, R. D., Goldman, R. D., Poirier, G. G., Kaufmann, S. H., and Earnshaw, W. C. (1996) Cleavage of lamin A by Mch2α but not CPP32: multiple interleukin 1β-converting enzyme-related proteases with distinct substrate recognition properties are active in apoptosis. *Proc. Natl. Acad. Sci. U.S.A.* **93,** 8395–8400
32. Walsh, J. G., Cullen, S. P., Sheridan, C., Lüthi, A. U., Gerner, C., and Martin, S. J. (2008) Executioner caspase-3 and caspase-7 are functionally distinct proteases. *Proc. Natl. Acad. Sci. U.S.A.* **105,** 12815–12819
33. Iglesias-Guimarais, V., Gil-Guiñon, E., Sánchez-Osuna, M., Casanelles, E., García-Belinchon, M., Comella, J. X., and Yuste, V. J. (2013) Chromatin collapse during caspase-dependent apoptotic cell death requires DNA fragmentation factor, 40-kDa subunit-/caspase-activated deoxyribonuclease-mediated 3′-OH single-strand DNA breaks. *J. Biol. Chem.* **288,** 9200–9215
34. Perez-Alvarez, S., Iglesias-Guimarais, V., Solesio, M. E., Melero-Fernandez de Mera, R. M., Yuste, V. J., Galindo, M. F., and Jordán, J. (2011) Methadone induces CAD degradation and AIF-mediated necrotic-like cell death in neuroblastoma cells. *Pharmacol. Res.* **63,** 352–360
35. Toné, S., Sugimoto, K., Tanda, K., Suda, T., Uehira, K., Kanouchi, H., Samejima, K., Minatogawa, Y., and Earnshaw, W. C. (2007) Three distinct stages of apoptotic nuclear condensation revealed by time-lapse imaging, biochemical and electron microscopy analysis of cell-free apoptosis. *Exp. Cell Res.* **313,** 3635–3644
36. Zhang, J., Wang, X., Bove, K. E., and Xu, M. (1999) DNA fragmentation factor 45-deficient cells are more resistant to apoptosis and exhibit different dying morphology than wild-type control cells. *J. Biol. Chem.* **274,** 37450–37454
37. Widlak, P. (2000) The DFF40/CAD endonuclease and its role in apoptosis. *Acta Biochim. Polon.* **47,** 1037–1044
38. Samejima, K., Toné, S., Kottke, T. J., Enari, M., Sakahira, H., Cooke, C. A., Durrieu, F., Martins, L. M., Nagata, S., Kaufmann, S. H., and Earnshaw, W. C. (1998) Transition from caspase-dependent to caspase-independent mechanisms at the onset of apoptotic execution. *J. Cell Biol.* **143,** 225–239
39. Sahara, S., Aoto, M., Eguchi, Y., Imamoto, N., Yoneda, Y., and Tsujimoto, Y. (1999) Acinus is a caspase-3-activated protein required for apoptotic chromatin condensation. *Nature* **401,** 168–173
40. Joselin, A. P., Schulze-Osthoff, K., and Schwerk, C. (2006) Loss of acinus inhibits oligonucleosomal DNA fragmentation but not chromatin condensation during apoptosis. *J. Biol. Chem.* **281,** 12475–12484
41. Widlak, P., Palyvoda, O., Kumala, S., and Garrard, W. T. (2002) Modeling apoptotic chromatin condensation in normal cell nuclei: requirement for intranuclear mobility and actin involvement. *J. Biol. Chem.* **277,** 21683–21690
42. Majczak, A., Karbowski, M., Kaminski, M., Masaoka, M., Kurono, C., Niemczyk, E., Kedzior, J., Soji, T., Knap, D., Hallmann, A., and Wakabayashi, T. (2004) Modification of physicochemical properties of actin filaments suppresses cell fragmentation in the execution phase of staurosporine-induced apoptotic processes. *J. Electron Microsc.* **53,** 635–647
43. Dini, L., Coppola, S., Ruzittu, M. T., and Ghibelli, L. (1996) Multiple path-

ways for apoptotic nuclear fragmentation. *Exp. Cell Res.* **223,** 340–347
44. Kasibhatla, S., and Tseng, B. (2003) Why target apoptosis in cancer treatment? *Mol. Cancer Ther.* **2,** 573–580
45. de Bruin, E. C., and Medema, J. P. (2008) Apoptosis and non-apoptotic deaths in cancer development and treatment response. *Cancer Treat. Rev.* **34,** 737–749
46. Ermakov, A. V., Konkova, M. S., Kostyuk, S. V., Izevskaya, V. L., Baranova, A., and Veiko, N. N. (2013) Oxidized extracellular DNA as a stress signal in human cells. *Oxid. Med. Cell. Longev.* **2013,** 649747
47. Glebova, K., Veiko, N., Kostyuk, S., Izhevskaya, V., and Baranova, A. (2013) Oxidized extracellular DNA as a stress signal that may modify response to anticancer therapy. *Cancer Lett.* 10.1016/j.canlet. 2013.09.005